Theory of interactions between cavity photons induced by a mesoscopic circuit

Audrey Cottet,[1] Zaki Leghtas,[2,1] and Takis Kontos[1]
[1]*Laboratoire de Physique de l'Ecole normale supérieure, ENS, Université PSL, CNRS, Sorbonne Université, Université de Paris, F-75005 Paris, France*
[2]*Centre Automatique et Systèmes, Mines-ParisTech, PSL Research University, 60, Boulevard Saint-Michel, 75006 Paris, France*

(Received 11 October 2019; revised 24 June 2020; accepted 9 September 2020; published 5 October 2020)

We use a quantum path-integral approach to describe the behavior of a microwave cavity coupled to a dissipative mesoscopic circuit. We integrate out the mesoscopic electronic degrees of freedom to obtain a cavity effective action at fourth order in the light/matter coupling. By studying the structure of this action, we establish sufficient conditions in which the cavity dynamics can be described with a Lindblad equation. This equation depends on effective parameters set by electronic correlation functions. It reveals that the mesoscopic circuit induces an effective Kerr interaction and two-photon dissipative processes. We use our method to study the effective dynamics of a cavity coupled to a double quantum dot with normal metal reservoirs. If the cavity is driven at twice its frequency, the double-dot circuit generates photonic squeezing and nonclassicalities visible in the cavity Wigner function. In particular, we find a counterintuitive situation where mesoscopic dissipation enables the production of photonic Schrödinger cats. These effects can occur for realistic circuit parameters. Our method can be generalized straightforwardly to more complex circuit geometries with, for instance, multiple quantum dots and other types of fermionic reservoirs such as superconductors and ferromagnets.

DOI: 10.1103/PhysRevB.102.155105

I. INTRODUCTION

Embedding nonlinear Josephson circuits into microwave cavities has enabled impressive progress in the quantum control of microwave light [1]. Indeed, the field of circuit quantum electrodynamics (QED) offers many functionalities. For instance, squeezed photonic states, where the uncertainty of one quadrature is reduced below the zero-point level, can be obtained by embedding a nonlinear circuit such as a superconducting quantum interference device (SQUID) array into a microwave cavity [2]. A classical cavity state can evolve into a quantum superposition of coherent states due to an effective Kerr interaction provided by a superconducting quantum bit [3]. One can also generate arbitrary quantum superpositions of Fock states by using the time-dependent coupling of a superconducting qubit to a microwave resonator [4,5]. For most quantum protocols implemented so far, cavity damping is a spurious effect. However, it has been demonstrated experimentally that in a nonlinear circuit QED setup driven with microwaves, photon-number dependent losses can be used to prepare photonic Schrödinger cat states [6,7] and stabilize autonomously Fock states [8]. This result contributes to a research field called "reservoir engineering," which promotes the idea that, contrary to common belief, dissipation is not always harmful for the quantumness of a system [9–12]. Thanks to this rich phenomenology, nonlinear microwave cavities offer many possibilities of applications, from sensing to quantum information and communication. For example, squeezed states of light offer a powerful resource for quantum-enhanced sensing [13,14]. More recently, quantum computing schemes have been suggested, where quantum information would be encoded in a manifold of cavity states stabilized autonomously by two-photon dissipation [15]. In this context, the photonic Wigner function is a widely measured quantity to characterize the joint statistics of the cavity field quadratures [16]. It is obtained experimentally by performing the cavity tomography [5].

In standard circuit QED experiments, the Josephson circuits coupled to microwave cavities are exclusively made of superconducting metals and Josephson junctions. However, due to the versatility of microwave fabrication techniques, the connection between circuit QED and mesoscopic physics is naturally growing [17,18]. Recently, circuits enclosing a single [19] or a double [20] quantum dot and normal [19,20], ferromagnetic [21,22], or superconducting reservoirs [23,24] have been coupled to microwave cavities. In the experiments performed so far, microwave cavities have appeared as a powerful means to characterize the electronic spectrum and dynamics of mesoscopic circuits. However, the scope of mesoscopic QED could go far beyond. Indeed, mesoscopic circuits are intrinsically nonlinear due to their anharmonic energy spectrum. Besides, fermionic reservoirs represent a specific source of dissipation which involves electrically controlled quantum transport. It is therefore appealing to investigate the potentialities of mesoscopic QED for producing quantum cavity states. In this direction, entangled light/matter states due to a strong charge/photon [24–26] or spin/photon [22,27–29] coupling have been obtained in recent experiments, using double quantum dot circuits. However, many more situations remain to be explored.

On the theory side, the effect of dissipative fermionic reservoirs in mesoscopic QED setups has been mostly investigated in the semiclassical regime where the number of cavity photons is so large that quantum fluctuations in the

 ©2020 American Physical Society

photon number can be disregarded [23,30–33]. Otherwise, a sequential tunneling description of quantum transport has been used, which is valid only for very small tunnel rates [34–39]. A general quantum description of mesoscopic QED is lacking. One needs to develop a theory which describes the cavity quantum dynamics in the presence of dissipative mesoscopic transport. This description must apply to complex circuit configurations with arbitrary tunnel couplings to voltage-biased fermionic reservoirs. It is also important to take into account the nonlinear photonic effects inherited from the light/matter interactions, which have not been included so far in the theory of mesoscopic QED and which offer a vast field of investigation. This requires to work beyond the second-order treatment of the light/matter coupling.

In this work, we fill these gaps by employing a quantum path-integral technique along the Keldysh contour, which is particularly convenient to integrate out electronic degrees of freedom and obtain an effective description of the cavity nonlinear behavior [40]. We consider a cavity with frequency ω_0 coupled to a mesoscopic circuit and excited with a microwave tone at frequency $2\omega_0$ with a moderate amplitude ε_p (i.e., ε_p can be treated to first order). We note g is the order of magnitude of the light/matter coupling in the mesoscopic QED device. We expand the effective quantum action of the cavity up to fourth order in the light/matter coupling. The expansion parameter is described in Appendix H, and for conciseness, is hereafter referred to as g. The cavity effective action depends on electronic correlation functions of the mesoscopic circuit, which we express in terms of Keldysh Green's functions. It reveals that the cavity is subject to photon-photon interactions mediated by the mesoscopic circuit. We establish sufficient conditions on mesoscopic correlators for having a description of the cavity dynamics with a Lindblad equation. In this case, the $2\omega_0$ drive produces, at third order in g, a coherent two-photon drive [41] and a less usual dissipative squeezing process [42,43]. Additionally, the mesoscopic circuit induces, at fourth order in g, Kerr photon-photon interaction as well as stochastic two-photon losses and gains. Importantly, our results are valid for tunnel couplings rates to the reservoirs of the mesoscopic circuit smaller as well as larger than the electronic temperature since no sequential tunneling hypothesis is required. We make the realistic assumption that the cavity has a large quality factor and a dressed linewidth much smaller than the mesoscopic resonances linewidth. We finally disregard Coulomb interactions in the mesoscopic circuit.

We use our method to study the quantum dynamics of a microwave cavity coupled to a noninteracting double quantum dot (DQD) with normal metal contacts biased with a voltage V_b (see Fig. 1). We identify two situations where the effective dynamics of the cavity is described by a Lindblad equation, which includes nonlinear light/matter interaction effects. The first situation is the limit of a low light/matter coupling ($g \approx 0.01\omega_0$). In this case, we derive an effective Lindblad equation description of the cavity behavior to third order in g, from which we obtain an analytic expression of the cavity Wigner function in stationary conditions. The $2\omega_0$ drive produces a coherent injection and/or withdrawal of photon pairs in the cavity [41] and a less usual squeezing dissipative process [42,43]. This leads to a squeezing of the cavity vacuum, which depends nontrivially on the system parameters [44–46]. The

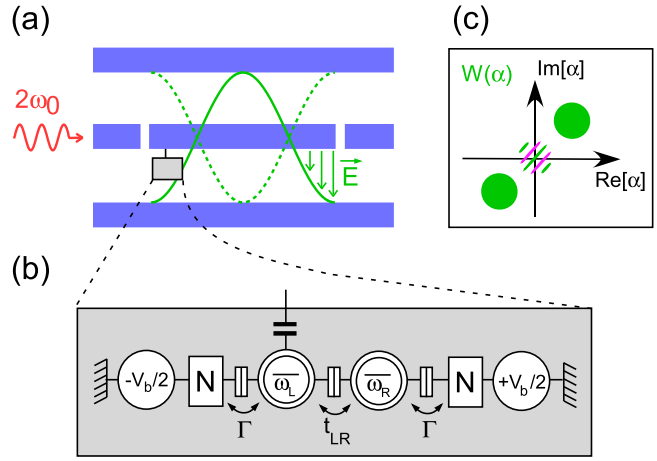

FIG. 1. Example of mesoscopic QED device. (a) Microwave cavity ac driven at twice the cavity frequency ω_0. The nanocircuit (in gray) is coupled capacitively to the cavity central conductor at an electric field node. (b) Double quantum dot coupled to normal metal reservoirs N with a tunnel rate Γ. The dots are tunnel coupled with a hopping strength t_{LR}. The normal metal reservoirs have a voltage bias V_b. (c) Schematic representation of the cavity Wigner function as a function of the field quadratures, measured by performing the cavity tomography.

second Lindbladian situation is when the double dot is resonant with $2\omega_0$ and has moderate interdot hopping and tunnel couplings to its reservoirs, and the light/matter coupling is moderate ($g \approx 0.1\omega_0$). In this case, a description to fourth order in g is necessary to describe the cavity dynamics. In this limit, we find that, in the absence of a cavity drive ($\varepsilon_p = 0$), dissipative transport in the double dot circuit can enable the stochastic absorption and/or emission of photon pairs in the cavity, depending on the value of V_b. When the cavity is ac driven ($\varepsilon_p \neq 0$) with $V_b = 0$, we show, with numerical simulations of the photonic Lindblad equation, that the DQD circuit can be used to produce photonic Schrödinger cat states. This effect is expected for realistic circuit parameters. It is due to a combination of the two-photon drive in $\varepsilon_p g^3/\omega_0^3$ and the photon pair damping in g^4/ω_0^3. Hence, counterintuitively, mesoscopic dissipation enables the generation of a quantum superposition of cavity states. In the same vein, recent experiments with Josephson circuits have shown that the combination of a two-photon drive with a Kerr photon-photon interaction [47–49] or two-photon losses [6,50] can be used to prepare autonomously Schrödinger cat states and protect these against some types of decoherence. This represents an important research direction in the context of the development of a bosonic encoding of quantum information with autonomous quantum error correction. Our work suggests that mesoscopic QED devices could offer interesting possibilities in this context.

Thanks to its generality, our approach could be used to explore many more circuit geometries and protocols. One can consider circuits with single [19] or multiple quantum dots [20]. One can also consider extended nanoconductors such as nanowires with a strong-orbit coupling, which raise a lot of attention in the search for Majorana quasiparticles [51–56] and which have been recently coupled to microwave cavities [57]. For this purpose, the nanoconductor can be

discretized into various internal sites by using a Hubbard model [31,33,58–60]. Finally, different types of fermionic reservoirs can be considered, such as normal metals [19,20], ferromagnets [21,22], or superconductors [23,24]. These mesoscopic QED devices could find applications in quantum information science, with, for instance, spin quantum bits [22,27–29] and Cooper pair splitters [61–63]; in quantum optics, with, for instance, lasing generated by mesoscopic circuits [34,64,65]; and also in condensed matter science, with the simulation of the Kondo effect in quantum dots [66] and the simulation of Anderson-Holstein problem [67]. Our approach could be instrumental for the study of these many configurations in the nonlinear quantum regime.

This article is organized as follows. Section II introduces the mesoscopic QED Hamiltonian and discusses a direct density matrix description of mesoscopic QED and its drawbacks. Section III presents the general description of mesoscopic QED with the path-integral approach. It also explains how the cavity effective action leads to a Lindblad description, at third order in g for any parameters, or at fourth order in g provided some mesoscopic correlation functions fulfill a Lindbladian condition. Section IV applies the results of Sec. III to the example of a microwave cavity coupled to a double quantum dot with normal metal contacts. In particular, it shows how the double dot can be used to squeeze the cavity vacuum or to produce photonic Schrödinger cats. Section V puts ours results in perspective with other recent works and Sec. VI concludes. Appendix A gives details on the derivation of the cavity effective action at fourth order in g. Appendix B 1 gives a direct calculation of the possible semiclassical values of the cavity photonic amplitude at fourth order in g (without using the path-integral approach). This enables a semiclassical interpretation of some of the parameters which occur in the cavity effective action. Appendix B 2 shows an alternative way to determine the possible semiclassical values of the cavity photonic amplitude, by considering the saddle points of the cavity action. The agreement between the results of Appendixes B 1 and B 2 at fourth order in g provides an important sanity check for our approach. Appendix C explains how to derive the action associated to a Lindblad equation. Appendix D establishes a quantitative equivalence at order 2 in g between the Lindblad equation arising from a direct density matrix approach and the Lindblad equation arising from the path-integral approach. Appendix E gives details on the calculation of the cavity Wigner function. Appendix F gives details on the dependence of the photonic squeezing effect on the double dot parameters. Appendix G gives a simple analytical expression of the linear charge susceptibility of a mesoscopic circuit (i.e., to second order in g) in the sequential tunneling limit to illustrate the regularization of our description by dissipative tunneling. Finally, Appendix H shows the calculation of the generalized charge susceptibilities of the mesoscopic circuit up to eighth order in g. This serves as a basis for discussing the regime of validity of our approach at fourth order in g. One needs sufficiently large tunneling rates to the fermionic reservoirs of the circuit on top of a small enough coupling g and cavity drive ε_p. It is difficult to give a simple analytic criterion for delimiting this regime. However, the evaluation of higher order charge susceptibilities given in Appendix H represents a suitable numerical check for the validity of our development.

II. DESCRIPTION OF MESOSCOPIC QED WITH A DIRECT DENSITY MATRIX APPROACH

A. System Hamiltonian

We consider a cavity with bare frequency ω_0 excited by a microwave drive $\varepsilon_{ac}(t)$ and coupled to a mesoscopic circuit. This circuit contains N discrete orbitals with index d, coupled to fermionic reservoirs with a continuum of states with index k. The mesoscopic circuit can be, for instance, a quantum dot circuit, in which case the orbitals d are located in the dots [18–20]. Each orbital d is coupled to the electric quadrature of the cavity field with a constant g_d (see Ref. [68] for a first-principles description of this effect and a microscopic expression of g_d). The resulting mesoscopic QED device can be described with the Hamiltonian

$$\hat{H}_{\rm tot} = \omega_0 \hat{a}^\dagger \hat{a} + \varepsilon_{ac}(t)(\hat{a}^\dagger + \hat{a}) + \hat{h}_b + \hat{H}_{\rm meso} + \sum_d g_d (\hat{a}^\dagger + \hat{a}) \hat{c}_d^\dagger \hat{c}_d \tag{1}$$

with

$$\hat{H}_{\rm meso} = \sum_d \omega_d \hat{c}_d^\dagger \hat{c}_d + \sum_{d<d'} (t_{d',d} \hat{c}_{d'}^\dagger \hat{c}_d + \text{H.c.}) + \sum_{k,d} \left(t_{k,d} \hat{c}_k^\dagger \hat{c}_d + \text{H.c.}\right) + \sum_k \omega_k \hat{c}_k^\dagger \hat{c}_k. \tag{2}$$

Above, $\hat{a}^\dagger$ is the cavity photon creation operator, $\hat{c}_d^\dagger$ is the electron creation operator in the discrete orbital $d \in [1, N]$, and $\hat{c}_k^\dagger$ is an electron creation operator in a level k of one of the fermionic reservoirs. In the general case, the indices k and d include the spin degree of freedom. We do not specify the exact mesoscopic circuit geometry for the moment. The tunnel hopping strength between two orbitals d and $d'[k]$ located in neighboring sites of the circuit is noted $t_{d'[k],d}$. We use $\hbar = 1$. Intrinsic cavity damping is described by the Hamiltonian $\hat{h}_b$, which we do not specify here. In most cases, the orbital energy ω_d of site d can be finely tuned with an electrostatic gate, and bias voltages can be applied to the fermionic reservoirs to induce electronic transport. Note that we disregard the coupling between the cavity field and the reservoirs levels k. This is relevant for most mesoscopic QED experiments where the coupling between discrete internal levels d and the cavity field is dominant due to the use of ac gates which connect levels d to the cavity central conductor. In the following, we assume that an ac drive

$$\varepsilon_{ac}(t) = (\varepsilon_p e^{-i2\omega_0 t} + \varepsilon_p^* e^{i2\omega_0 t})/2 \tag{3}$$

is applied to the cavity. We will see that both components in $e^{-i2\omega_0 t}$ and $e^{i2\omega_0 t}$ contribute to the the cavity response through higher order processes (effect in g^3 at least). For simplicity, we do not describe explicitly the microwave inputs and outputs of the cavity but this can be added straightforwardly by using the input/output theory [30,41,69].

B. Direct density matrix approach and its drawbacks

The most commonly used description of circuit QED is the density matrix approach, which consists in expressing directly the time evolution of the system density matrix. Here we will shortly discuss this approach to point out its weaknesses and

the interest of the path-integral approach in the context of nonlinear mesoscopic QED.

We assume that the light/matter interaction term is a perturbation in the system Hamiltonian, in comparison with the cavity contribution in ω_0 and mesoscopic contribution $\hat{H}_{\rm meso}$. For simplicity, in this section, we also assume that there is no cavity drive ($\varepsilon_p = 0$) and no cavity intrinsic dissipation (i.e., $\hat{h}_b$ is negligible). In these conditions, it is convenient to use the interaction picture, where the density matrix $\rho^I(t) = e^{i\omega_0\hat{a}^\dagger\hat{a}t + i\hat{H}_{\rm meso}t}\rho(t)e^{-i\omega_0\hat{a}^\dagger\hat{a}t - i\hat{H}_{\rm meso}t}$ of the full mesoscopic QED device (cavity + mesoscopic circuit) has an evolution equation

$$\frac{\partial\rho^I(t)}{\partial t} = -i[\hat{V}(t), \rho^I(t)] \tag{4}$$

with

$$\hat{V}(t) = \hat{N}(t)(\hat{a}e^{-i\omega_0 t} + \hat{a}^\dagger e^{i\omega_0 t}), \tag{5}$$

$$\hat{N}(t) = \sum_d g_d \hat{n}_d(t), \tag{6}$$

and

$$\hat{n}_d(t) = e^{i\hat{H}_{\rm meso}t}\hat{c}_d^\dagger\hat{c}_d e^{-i\hat{H}_{\rm meso}t}. \tag{7}$$

Note that $\hat{H}_{\rm meso}$ and $\hat{c}_d^\dagger\hat{c}_d$ do not commute due to dot-dot and dot-reservoir tunneling. Hence, from Eqs. (6) and (7), $\hat{N}(t)$ depends on time.

We now discuss the expression of the cavity dynamics at second order in g. The integration of Eq. (4) gives

$$\rho^I(t) = \rho^I(t_0) - i\int_{t_0}^t dt_1[V(t_1), \rho^I(t_1)] \tag{8}$$

with t_0 a reference time far in the past. Inserting this equation back in Eq. (4) gives

$$\frac{\partial\rho^I(t)}{\partial t} = -i[\hat{V}(t), \rho^I(t_0)] - \int_{t_0}^t dt_1[\hat{V}(t), [V(t_1), \rho^I(t_1)]]. \tag{9}$$

In the limit where the mesoscopic system has a correlation time τ which is much shorter than the cavity characteristic timescale of evolution T, only the times t_1 such that $t - t_1 \lesssim \tau$ will contribute in the above integral [70]. Accordingly, one can assume that the mesoscopic system is constantly at equilibrium, i.e.,

$$\rho^I(t_1) = \rho^0_{\rm meso} \otimes \rho^I_{\rm cav}(t_1), \tag{10}$$

with $\rho^0_{\rm meso}$ being the equilibrium density matrix of the mesoscopic circuit for $g_d = 0$. Finally, since $\tau \ll T$, one can use $\rho^I(t_1) = \rho^0_{\rm meso} \otimes \rho^I_{\rm cav}(t)$ in the above integral. Performing the trace $\underset{k,d}{\rm Tr}$ on the mesoscopic degrees of freedom, one finally gets

$$\begin{aligned}\frac{\partial\rho^I_{\rm cav}(t)}{\partial t} &= -i\underset{k,d}{\rm Tr}\big[\big[V(t), \rho^0_{\rm meso} \otimes \rho^I_{\rm cav}(t_0)\big]\big] \\ &\quad - \int_{t_0}^t dt_1 \underset{k,d}{\rm Tr}\big[\big[V(t), \big[V(t_1), \rho^0_{\rm meso} \otimes \rho^I_{\rm cav}(t)\big]\big]\big].\end{aligned} \tag{11}$$

If we keep only resonant terms and consider a stationary situation, a reorganization of Eq. (11) gives

$$\begin{aligned}\frac{\partial\rho^I_{\rm cav}(t)}{\partial t} &= -2\,{\rm Im}[\chi_B(\omega_0)]\mathcal{D}_{\hat{a}}\big(\rho^I_{\rm cav}(t)\big) \\ &\quad - 2\,{\rm Im}[\chi_A(\omega_0)]\mathcal{D}_{\hat{a}^\dagger}\big(\rho^I_{\rm cav}(t)\big) \\ &\quad - i\,{\rm Re}[\chi_B(\omega_0) - \chi_A(\omega_0)]\big[\hat{a}^\dagger\hat{a}, \rho^I_{\rm cav}(t)\big] + o(\check{g}^2).\end{aligned} \tag{12}$$

Above,

$$\mathcal{D}_{\hat{L}_j}\big(\rho^I_{\rm cav}\big) = \hat{L}_j\rho^I_{\rm cav}\hat{L}_j^\dagger - \tfrac{1}{2}\big\{\hat{L}_j^\dagger\hat{L}_j, \rho^I_{\rm cav}\big\} \tag{13}$$

is the Lindblad superoperator associated to the jump operator $\hat{L}_j$. We have disregarded the first-order term in g which is nonresonant with the cavity. The mesoscopic correlators

$$\chi_A(t) = -i\theta(t)\langle\hat{N}(0)\hat{N}(t)\rangle \tag{14}$$

and

$$\chi_B(t) = -i\theta(t)\langle\hat{N}(t)\hat{N}(0)\rangle \tag{15}$$

whose Fourier transforms $\chi_{A[B]}(\omega) = \int dt\,\chi_{A[B]}(t)e^{i\omega t}$ appear in Eq. (12) have to be evaluated to second order in the light/matter interaction. More precisely, from Eq. (6), one can use $\langle\hat{N}(t')\hat{N}(t)\rangle = \sum_{d,d'} g_d g_{d'} A_{d',d}(t',t)$ and $A_{d',d}(t',t) = \langle\hat{c}_{d'}^\dagger(t')\hat{c}_{d'}(t')\hat{c}_d^\dagger(t)\hat{c}_d(t)\rangle_0$, where $\langle\rangle_0$ denotes a statistical average calculated for $g_d = 0$ for any d, i.e., $A_{d',d}(t',t) = {\rm Tr}[\rho^0_{\rm meso}\hat{c}_{d'}^\dagger(t')\hat{c}_{d'}(t')\hat{c}_d^\dagger(t)\hat{c}_d(t)]$. In the absence of Coulomb interactions, the evaluation of $A_{d,d'}$ can be done straightforwardly by using the Wick theorem (see, for instance, Ref. [71]).

To describe the dynamics of $\rho^I_{\rm cav}$ beyond the second order in g, one straightforward idea is to start with Eq. (9) and iterate the substitution of $\rho^I(t)$ by the right member of Eq. (8). This gives

$$\begin{aligned}&\frac{\partial\rho^I_{\rm cav}(t)}{\partial t} \\ &= -i\underset{k,d}{\rm Tr}[[V(t), \rho^I(t_0)]] - \int_{t_0}^t dt_1 \underset{k,d}{\rm Tr}[[V(t), [V(t_1), \rho^I(t_0)]]] \\ &\quad + i\iint_{t_0,t_0}^{t,t_1} dt_1 dt_2 \underset{k,d}{\rm Tr}[[V(t), [V(t_1), [V(t_2), \rho^I(t_0)]]]] \\ &\quad + \iiint_{t_0,t_0,t_0}^{t,t_1,t_2} dt_1 dt_2 dt_3 \underset{k,d}{\rm Tr}[[V(t), \\ &\quad \times [V(t_1), [V(t_2), [V(t_3), \rho^I(t_3)]]]]].\end{aligned} \tag{16}$$

At this stage, conceptual difficulties as well as calculation heaviness make the generalization of Eq. (12) nontrivial. First, a backaction of the cavity on the mesoscopic density matrix should be taken into account. This means that expression (10) cannot be used to express $\rho^I(t_0)$ and $\rho^I(t_3)$ in Eq. (16). Hence, it will be more difficult to introduce independently defined mesoscopic correlators in the expression of $\partial\rho^I_{\rm cav}(t)/\partial t$. Besides, the dynamics of the system is not anymore Markovian in the general case, so that $\rho^I_{\rm cav}(t)$ does not appear naturally in the right member of Eq. (16). Finally, even in a case where a generalization of the Markovian Eq. (12) would be possible, due to the iterative structure of Eq. (16), the number

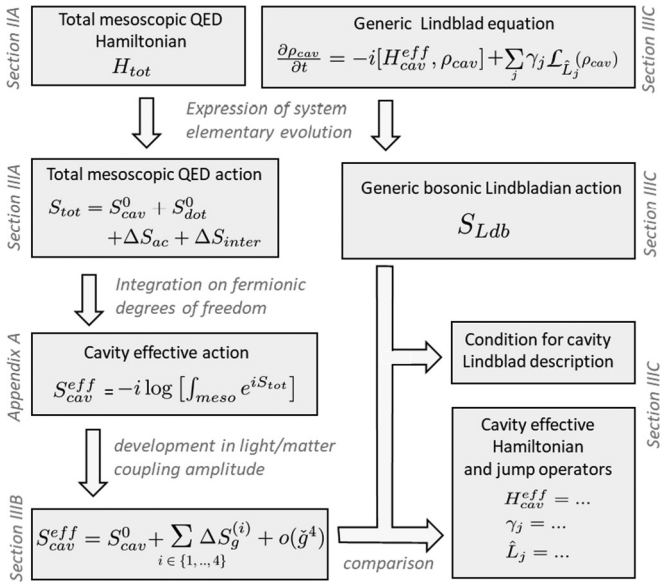

FIG. 2. Synoptic table of the theoretical approach introduced in Sec. III.

of mesoscopic correlators to define would explode, and the explicit calculation of these correlators from the mesoscopic circuit Hamiltonian would be a lengthy task. In fact, all these difficulties stem from the fact that the trace on the mesoscopic degrees of freedom is performed after the time evolution of $\rho^I(t)$ is expressed. It is thus crucial to use a calculation method where the electronic degrees of freedom are integrated earlier, i.e., at the level of the device Hamiltonian. This is why we will develop an efficient quantum path-integral description of mesoscopic QED in the next section.

III. GENERAL DESCRIPTION OF MESOSCOPIC QED WITH THE QUANTUM PATH-INTEGRAL FORMALISM

This section describes a general method based on the quantum path-integral description to describe the effective behavior of a microwave cavity coupled to a mesoscopic circuit. From the mesoscopic QED Hamiltonian of Eq. (1), we express the global quantum action of the system (see Sec. III A). The fermionic degrees of freedom in this action can be integrated out to obtain the cavity effective action (see Sec. III B). We compare this action to the action given by a generic Lindblad description of a cavity dynamics (see Sec. III C). This enables us to establish a criterion to have a cavity Lindblad dynamics at fourth order in the light/matter coupling. When this criterion is fulfilled, we can finally write the cavity effective Lindblad equation. This approach is summarized in the synoptic table of Fig. 2.

A. Quantum action of the whole mesoscopic QED device

A generic description of mesoscopic QED can be built by expressing the Schwinger-Keldysh partition function of the system with a quantum path integral along the Keldysh contour [40]. To this end, we define, along the forward and backward branches of the Keldysh contour, the fields $\varphi_\pm(t)$, $\bar{\varphi}_\pm(t)$, $\psi_{\pm,d}(t)$, and $\bar{\psi}_{\pm,d}(t)$, which correspond to a possible "realization" of the operators $\hat{a}$, $\hat{a}^\dagger$, $\hat{c}_d$, and $\hat{c}^\dagger_d$ over time [72]. It is convenient to define the average and relative field components $\varphi_{cl/q}(t) = [\varphi_+(t) \pm \varphi_-(t)]/\sqrt{2}$, $\bar{\varphi}_{cl/q}(t) = [\bar{\varphi}_+(t) \pm \bar{\varphi}_-(t)]/\sqrt{2}$, $\psi_{0/1,d}(t) = [\psi_{+,d}(t) \pm \psi_{-,d}(t)]/\sqrt{2}$, and $\bar{\psi}_{0/1,d}(t) = [\bar{\psi}_{+,d}(t) \mp \bar{\psi}_{-,d}(t)]/\sqrt{2}$. These quantities can be grouped into vectorial fields $\varphi(t) = {}^t\{\varphi_{cl}(t), \varphi_q(t)\}$, $\bar{\varphi}(t) = \{\bar{\varphi}_{cl}(t), \bar{\varphi}_q(t)\}$, $\psi(t) = {}^t\{\psi_0(t), \psi_1(t)\}$, and $\bar{\psi}(t) = \{\bar{\psi}_0(t), \bar{\psi}_1(t)\}$. Note that in the case of a mesoscopic circuit with several discrete orbitals, the fields $\psi_0(t)$ and $\psi_1(t)$ have an orbital structure $\psi_m(t) = {}^t\{\psi_{m,d_1}(t), \ldots, \psi_{m,d_N}(t)\}$ with $m \in \{0/1\}$. In the main text of this article, all the fields have a time argument t, which is omitted for brevity, except when two times t and t' are involved in an equation. The global Schwinger-Keldysh partition function Z of the mesoscopic QED device and the corresponding quantum action $S_{\rm tot}$ can be obtained directly from Hamiltonian (1) by considering the elementary evolution of the system along the Keldysh contour [40]. This gives

$$Z = \int d[\bar{\varphi}, \varphi, \bar{\psi}, \psi] e^{iS_{\rm tot}(\bar{\varphi}, \varphi, \bar{\psi}, \psi)} \tag{17}$$

with

$$S_{\rm tot}(\bar{\varphi}, \varphi, \bar{\psi}, \psi) = S^0_{\rm cav}(\bar{\varphi}, \varphi) + S^0_{\rm meso}(\bar{\psi}, \psi) + \Delta S_{ac}(\bar{\varphi}, \varphi) + \Delta S_{\rm inter}(\bar{\varphi}, \varphi, \bar{\psi}, \psi). \tag{18}$$

Above, $d[\bar{\varphi}, \varphi, \bar{\psi}, \psi]$ is the differential element associated to the fields $\bar{\varphi}$, φ, $\bar{\psi}$, and ψ. The term

$$S^0_{\rm cav}(\bar{\varphi}, \varphi) = \int_t [\bar{\varphi}_{cl} \quad \bar{\varphi}_q] \begin{bmatrix} 0 & D_t - \frac{i\Lambda_0}{2} \\ D_t + \frac{i\Lambda_0}{2} & i\Lambda_0(1 + 2n_B) \end{bmatrix} \begin{bmatrix} \varphi_{cl} \\ \varphi_q \end{bmatrix} \tag{19}$$

is the bare cavity action, with $D_t = i\partial t - \omega_0$, $n_B = 1/(e^{\omega_0/k_B T} - 1)$, and Λ_0, a damping rate due to the cavity bath treated in the Markovian approximation [73]. For compactness, we note $\int_{-\infty}^{+\infty} dt = \int_t$. The cavity drive brings a contribution

$$\Delta S_{ac}(\bar{\varphi}, \varphi) = -\sqrt{2} \int_t (\bar{\varphi}_q + \varphi_q) \varepsilon_{ac}(t). \tag{20}$$

The bare action from the mesoscopic circuit is

$$S^0_{\rm meso}(\bar{\psi}, \psi) = \int_{t,t'} \bar{\psi}(t) \check{G}^{-1}(t, t') \psi(t') \tag{21}$$

with $\check{G}$ being the mesoscopic circuit Green's function in the absence of light/matter coupling. The contribution from the light/matter coupling is

$$\Delta S_{\rm inter}(\bar{\varphi}, \varphi, \bar{\psi}, \psi) = -\int_{t,t'} \bar{\psi}(t) [\check{v}(\bar{\varphi}, \varphi, t) \delta(t - t')] \psi(t') \tag{22}$$

with $\iint_{-\infty}^{+\infty} dt\, dt' = \int_{t,t'}$ and $\check{v}$ being a light/matter coupling function. Both $\check{G}$ and $\check{v}$ are defined below.

The unperturbed mesoscopic circuit Green's function which appears in Eq. (21) has the structure $\check{G}(t, t') =$

$\int_\omega \check{G}(\omega)e^{i\omega(t'-t)}$ with [40]

$$\check{G}(\omega) = \begin{bmatrix} \tilde{G}_r(\omega) & \tilde{G}_K(\omega) \\ \tilde{0} & \tilde{G}_a(\omega) \end{bmatrix} \tag{23}$$

in the 2×2 mesoscopic Keldysh space. Above, $\tilde{0}$ is a matrix full of zeros in the $N \times N$ the mesoscopic orbitals space. The retarded, advanced, and Keldysh components $\tilde{G}_{r/a/K}(\omega)$ of $\check{G}$ also have a $N \times N$ structure in the mesoscopic orbital space. In the absence of superconducting correlations in a circuit, the elements of $\tilde{G}_r$, $\tilde{G}_a$, and $\tilde{G}_K$ in the line d and column d' can be defined as

$$G_r^{d,d'}(t,t') = -i\theta(t)\langle\{\hat{c}_d(t), \hat{c}_{d'}^\dagger(t')\}\rangle, \tag{24}$$

$$G_a^{d,d'}(t,t') = i\theta(-t)\langle\{\hat{c}_d(t), \hat{c}_{d'}^\dagger(t')\}\rangle, \tag{25}$$

and

$$G_K^{d,d'}(t,t') = -i\langle[\hat{c}_d(t), \hat{c}_{d'}^\dagger(t')]\rangle, \tag{26}$$

respectively. We also use the stationary relations $\tilde{G}_{r/a/K}(t,t') = \int_\omega \tilde{G}_{r/a/K}(\omega)e^{i\omega(t'-t)}$. Importantly, the index $d \in [1, N]$ in the above Green's functions runs only on the set of confined discrete orbitals of the mesoscopic circuit (like, for instance, quantum dot orbitals) which remain after the leads' orbital continua have been integrated out. The leads contribute to $\check{G}$ through self-energy terms which depend on the tunnel rates between the mesoscopic orbitals d and the leads. At this stage, we do not give a more explicit expression for $\check{G}$ because we consider a generic mesoscopic circuit. An example of expression for $\check{G}$ will be given in Sec. IV for a noninteracting double dot [see Eqs. (72)–(74)].

The light matter coupling occurs in Eq. (22) through the term

$$\check{v}(\bar{\varphi}, \varphi, t) = \check{g}\frac{[\bar{\varphi}_{cl}(t) + \varphi_{cl}(t)]\check{\sigma}_0 + [\bar{\varphi}_q(t) + \varphi_q(t)]\check{\sigma}_1}{\sqrt{2}}. \tag{27}$$

Above, we use matrices $\check{\sigma}_{0[1]} = \mathring{\sigma}_{0[1]} \otimes \widetilde{1}$, where $\mathring{\sigma}_0$ and $\mathring{\sigma}_1$ correspond to the identity and the first Pauli matrix in the Keldysh subspace of the mesoscopic circuit (index 0/1) and $\widetilde{1}$ is the identity in the mesoscopic orbitals subspace. We also note $\check{g} = \mathring{\sigma}_0 \otimes \tilde{g}$ with $\tilde{g} = diag[g_1, \ldots, g_N]$, a diagonal matrix in the mesoscopic orbitals subspace. More generally, the superscripts $\circ$ and $\sim$ decorate a matrix in the 2×2 mesoscopic Keldysh subspace and the $N \times N$ mesoscopic orbital subspace, respectively. The superscript $\vee$ decorates a matrix in the tensor product of these two spaces. The notation g used previously corresponds to $g = \max_d[g_d]$.

B. Effective cavity action to fourth order in g

In order to obtain an effective description of the cavity dynamics solely, one must integrate out the electronic degrees of freedom in Eq. (17). For simplicity, we will disregard Coulomb interactions in the mesoscopic circuit. In this case, the mesoscopic QED action is quadratic with respect the electronic fields ψ and $\bar{\psi}$, and one can thus perform a straightforward Gaussian integration of Eq. (17) on these fields (in the interacting case, it is possible to use more elaborate integration procedures [40]). The resulting effective cavity action $S_{\rm cav}^{\rm eff}(\bar{\varphi}, \varphi)$ can be simplified after a systematic expansion with respect to the light/matter coupling matrix $\check{g}$ (see Appendix A for details). We work to fourth order in g in order to capture essential nonlinear electron/photon interaction effects. In order to simplify the final expression of $S_{\rm cav}^{\rm eff}$, we assume that the dressed cavity linewidth is much smaller than ω_0 and the width of the mesoscopic resonances linewidth. This criterion is largely satisfied in experiments as well as for the parameters used in this paper. We finally obtain the expression

$$S_{\rm cav}^{\rm eff}(\bar{\varphi}, \varphi) = S_{\rm cav}^0(\bar{\varphi}, \varphi) + \sum_{i\in\{2,3,4\}} \Delta S_g^{(i)}(\bar{\varphi}, \varphi) + o(\check{g}^4). \tag{28}$$

Above, $\Delta S_g^{(i)}$ is the mesoscopic circuit contribution to $S_{\rm cav}^{\rm eff}$ to i^{th} order in g. The first order contribution in g can be disregarded because it is not resonant with the cavity [see Eqs. (A13) and (A14) of Appendix A].

The second-order contribution

$$\Delta S_g^{(2)}(\bar{\varphi}, \varphi) = -\int_t [\bar{\varphi}_{cl} \quad \bar{\varphi}_q].\begin{bmatrix} 0 & \chi_2^* \\ \chi_2 & \lambda_2 \end{bmatrix}.\begin{bmatrix} \varphi_{cl} \\ \varphi_q \end{bmatrix} \tag{29}$$

involves the semiclassical charge susceptibility

$$\chi_2 = -\frac{i}{2}\int_\omega \mathop{\rm Tr}_d[\tilde{G}_K(\omega)\tilde{g}(\tilde{G}_a(\omega - \omega_0) + \tilde{G}_r(\omega + \omega_0))\tilde{g}] \tag{30}$$

of the mesoscopic circuit at frequency ω_0 and the correlation function

$$\lambda_2 = -\frac{i}{2}\int_\omega \mathop{\rm Tr}_d[\tilde{G}_K(\omega)\tilde{g}\tilde{G}_K(\omega + \omega_0)\tilde{g} + \tilde{G}_a(\omega)\tilde{g}\tilde{G}_r(\omega + \omega_0)\tilde{g} + \tilde{G}_r(\omega)\tilde{g}\tilde{G}_a(\omega + \omega_0)\tilde{g}]. \tag{31}$$

We note $\int_\omega = \int_{-\infty}^{+\infty} \frac{d\omega}{2\pi}$, and $\mathop{\rm Tr}_d$ is the trace operator on the mesoscopic orbital index d. Note that χ_2 has already been introduced in other works [23,30–33,39,74], essentially for studying the semiclassical behavior of a mesoscopic QED device to second order in g. A cavity frequency shift is caused by $\mathrm{Re}[\chi_2]$, whereas $\mathrm{Im}[\chi_2]$ renormalizes the bare cavity linewidth Λ_0 of Eq. (19). The parameter λ_2 is necessary to describe the quantum regime of mesoscopic QED, but it has been disregarded so far. From Eq. (31) with $\tilde{G}_K(\omega) = -\tilde{G}_K(\omega)^\dagger$ and $\tilde{G}_a(\omega) = \tilde{G}_r(\omega)^\dagger$, one can check that λ_2 is purely imaginary.

For $\varepsilon_p \neq 0$, we obtain a third-order term $S_g^{(3)}(t)$ in g which can be expressed as

$$\begin{aligned}\Delta S_g^{(3)}(\bar{\varphi}, \varphi) &= -i\int_t e^{-2i\omega_0 t}[\bar{\varphi}_{cl} \quad \bar{\varphi}_q].\begin{bmatrix} 0 & U_{cl}/2 \\ U_{cl}/2 & U_q \end{bmatrix}.\begin{bmatrix} \bar{\varphi}_{cl} \\ \bar{\varphi}_q \end{bmatrix} \\ &\quad - i\int_t e^{2i\omega_0 t}[\varphi_{cl} \quad \varphi_q].\begin{bmatrix} 0 & -U_{cl}^*/2 \\ -U_{cl}^*/2 & U_q^* \end{bmatrix}.\begin{bmatrix} \varphi_{cl} \\ \varphi_q \end{bmatrix}\end{aligned} \tag{32}$$

with

$$\begin{aligned}U_{cl} = -\frac{\beta_p}{2}\int_\omega (&\mathop{\rm Tr}_{k,d}[\check{\sigma}_1\check{g}\check{G}(\omega)\check{g}\check{G}(\omega + \omega_0)\check{g}\check{G}(\omega - \omega_0)] \\ &+ \mathop{\rm Tr}_{k,d}[\check{G}(\omega)\check{\sigma}_1\check{g}\check{G}(\omega + \omega_0)\check{g}\check{G}(\omega - \omega_0)\check{g}]),\end{aligned} \tag{33}$$

$$U_q = -\frac{\beta_p}{2}\int_\omega \mathop{\rm Tr}_{k,d}[\check{\sigma}_1\check{g}\check{G}(\omega)\check{\sigma}_1\check{g}\check{G}(\omega + \omega_0)\check{g}\check{G}(\omega - \omega_0)] \tag{34}$$

and

$$\beta_p = \varepsilon_p t_0/2. \tag{35}$$

Above, we note $\underset{k,d}{\mathrm{Tr}}$ as the trace operator on both the mesoscopic orbital index d and the Keldysh index k. The prefactor

$$t_0 = \mathcal{G}_0^r(2\omega_0) + \mathcal{G}_0^a(-2\omega_0) \tag{36}$$

takes into account how the mesoscopic circuit feels the ac drive through the cavity, with

$$\mathcal{G}_0^{r/a}(\omega) = \left(\omega - \omega_0 \pm i\frac{\Lambda_0}{2}\right)^{-1} \tag{37}$$

being the bare cavity retarded/advanced Green's function [see Eq. (B3) for a semiclassical picture of this effect]. Subsequently, the reaction of the mesoscopic circuit to the ac drive affects the cavity effective behavior, as described by the terms in U_q and U_{cl}. Importantly, these terms can be significant because the smallness of t_0 can be compensated by the use of a sufficiently large drive amplitude β_p. Interestingly, the coefficient U_{cl} corresponds to the semiclassical joint response of the mesoscopic charge to the cavity field in $\hat{a}$ and to the drive in β_p [see Appendix B 1, Eq. (B7)].

Finally, we find a fourth-order contribution in g, which occurs even for $\beta_p = 0$, i.e.,

$$\Delta S_g^{(4)}(\bar{\varphi}, \varphi) = -\int_t [\bar{\varphi}_{cl}\bar{\varphi}_{cl} \quad \bar{\varphi}_{cl}\bar{\varphi}_q \quad \bar{\varphi}_q\bar{\varphi}_q] \cdot \mathcal{A} \cdot \begin{bmatrix} \varphi_{cl}\varphi_{cl} \\ \varphi_{cl}\varphi_q \\ \varphi_q\varphi_q \end{bmatrix} \tag{38}$$

with

$$\mathcal{A} = \begin{bmatrix} 0 & \chi_4^* & -U_4^* \\ \chi_4 & \lambda_4 & V_4^* \\ U_4 & V_4 & W_4 \end{bmatrix}, \tag{39}$$

$$\chi_4 = i(\mathcal{N}_{q,cl,cl,cl} + \mathcal{N}_{cl,q,cl,cl}), \tag{40}$$

$$\lambda_4 = i(\mathcal{N}_{cl,q,cl,q} + \mathcal{N}_{cl,q,q,cl} + \mathcal{N}_{q,cl,cl,q} + \mathcal{N}_{q,cl,q,cl}), \tag{41}$$

$$V_4 = i(\mathcal{N}_{q,q,cl,q} + \mathcal{N}_{q,q,q,cl}), \tag{42}$$

$$U_4(\omega_0) = i\mathcal{N}_{q,q,cl,cl}, \tag{43}$$

$$W_4(\omega_0) = i\mathcal{N}_{q,q,q,q}, \tag{44}$$

$$\mathcal{N}_{f,f',l,l'} = -\int_\omega \underset{k,d}{\mathrm{Tr}}\left[\frac{1}{8}\check{G}(\omega)\hat{\sigma}_f\check{g}\check{G}_+\hat{\sigma}_l\check{g}\check{G}(\omega)\hat{\sigma}_{f'}\check{g}\check{G}_+\hat{\sigma}_{l'}\check{g} + \frac{1}{4}\check{G}(\omega)\hat{\sigma}_f\check{g}\check{G}_+\hat{\sigma}_{f'}\check{g}\check{G}(\omega+2\omega_0)\hat{\sigma}_l\check{g}\check{G}_+\hat{\sigma}_{l'}\check{g}\right], \tag{45}$$

and $\check{G}_+ = \check{G}(\omega + \omega_0)$. Note that λ_4 and W_4 are purely imaginary due to $\tilde{G}_K(\omega) = -\tilde{G}_K(\omega)^\dagger$ and $\tilde{G}_a(\omega) = \tilde{G}_r(\omega)^\dagger$. The coefficient χ_4 corresponds to the second-order semiclassical response function of the quantum dot to the cavity electric field [see Appendix B 1, Eq. (B7)]. The other coefficients λ_4, U_4, V_4, and W_4 are necessary to describe quantum fluctuations of the cavity field. In summary, Eqs. (28)–(45) describe the effective action of a microwave cavity in a generic mesoscopic QED device to fourth order in the light/matter coupling. This requires us to introduce types of quantum dot correlators other than the known χ_2. We will discuss the physical effect of the correlators λ_2, U_{cl}, U_q, χ_4, λ_4, U_4, V_4, and W_4 in the next sections. Importantly, one has to choose an appropriate technique to obtain an explicit description of the cavity dynamics out of the cavity effective action. In the following, we will consider situations such that an effective Lindblad equation on the cavity density matrix can be used.

C. Correspondence between the cavity effective action and a photonic Lindblad equation

The most popular description of circuit QED is the Lindblad equation which describes the evolution of the cavity density matrix. Below, we come back to this description, already illustrated by our Eq. (12), to clarify the physical meaning of the different terms in the cavity action of Sec. III B.

1. Cavity effective Lindblad equation up to third order in g

In the limit of low couplings g_d and limited cavity drive β_p, the cavity field remains small so that one can truncate the cavity effective action to third order in g. In this case, we show below that it is always possible to establish a Lindblad equation on the cavity density matrix. Thereby, we clarify the physical meaning of the terms in U_{cl} and U_q.

When a cavity follows a Lindblad description, the time derivative of its density matrix $\rho_{\mathrm{cav}}(t)$ can be expressed as [16]

$$\frac{\partial \rho_{\mathrm{cav}}(t)}{\partial t} = -i\left[H_{\mathrm{cav}}^{\mathrm{eff}}, \rho_{\mathrm{cav}}(t)\right] + \sum_j \gamma_j \mathcal{D}_{\hat{L}_j}(\rho_{\mathrm{cav}}(t)) \tag{46}$$

with $H_{\mathrm{cav}}^{\mathrm{eff}}$ being the effective cavity Hamiltonian, γ_j being the rate of a dissipative process corresponding to the jump operator $\hat{L}_j$, and $\mathcal{D}_{\hat{L}_j}(\rho_{\mathrm{cav}})$ being defined in Eq. (13). Let us assume that the effective Hamiltonian has the generic form

$$H_{\mathrm{cav}}^{\mathrm{eff}} = (\omega_0 + \Delta\omega_0)\hat{a}^\dagger\hat{a} + i\rho_p e^{-i2\omega_0 t}\hat{a}^{\dagger 2} - i\rho_p^* e^{i2\omega_0 t}\hat{a}^2 \tag{47}$$

and the dissipative processes are characterized by $(\gamma_j, \hat{L}_j) \in \mathcal{P}$ with

$$\mathcal{P} = \{(\gamma_{\mathrm{loss}}, \hat{a}), (\gamma_{\mathrm{gain}}, \hat{a}^\dagger), (\gamma_p, \hat{a} + e^{i\varphi_p}e^{-i2\omega_0 t}\hat{a}^\dagger)\}. \tag{48}$$

The above real parameters $\Delta\omega_0$, ρ_p, γ_{loss}, γ_{gain}, γ_p, and φ_p are unspecified for the moment. The action corresponding to the master Eq. (46) can be expressed as (see details in Appendix C)

$$S_{\mathrm{Mark}}(t) = \int_t [\bar{\varphi}_{cl} \quad \bar{\varphi}_q].\begin{bmatrix} 0 & F_t - i\frac{\gamma_-}{2} \\ F_t + i\frac{\gamma_-}{2} & i\gamma_+ \end{bmatrix}.\begin{bmatrix} \varphi_{cl} \\ \varphi_q \end{bmatrix} + \int_t e^{-i2\omega_0 t}[\bar{\varphi}_{cl} \quad \bar{\varphi}_q].\begin{bmatrix} 0 & -i\rho_p \\ -i\rho_p & i\gamma_p e^{i\varphi_p} \end{bmatrix}.\begin{bmatrix} \bar{\varphi}_{cl} \\ \bar{\varphi}_q \end{bmatrix} + \int_t e^{i2\omega_0 t}[\varphi_{cl} \quad \varphi_q].\begin{bmatrix} 0 & i\rho_p^* \\ i\rho_p^* & i\gamma_p e^{-i\varphi_p} \end{bmatrix}.\begin{bmatrix} \varphi_{cl} \\ \varphi_q \end{bmatrix} \tag{49}$$

with

$$\gamma_- = \gamma_{\rm loss} - \gamma_{\rm gain}, \tag{50}$$

$$\gamma_+ = \gamma_{\rm loss} + \gamma_{\rm gain} + 2\gamma_p, \tag{51}$$

and $F_t = i\partial t - \omega_0 - \Delta\omega_0$. It is possible to perform an exact identification between the action of Eq. (49) and the cavity effective action to third order in g [i.e., Eqs. (29) + (32)] by using parameters $\Delta\omega_0$, ρ_p, $\gamma_{\rm loss}$, $\gamma_{\rm gain}$, γ_p, and φ_p given by the relations:

$$\Delta\omega_0 = {\rm Re}[\chi_2], \tag{52}$$

$$\rho_p = U_{cl}/2, \tag{53}$$

$$\gamma_p e^{i\varphi_p} = -U_q, \tag{54}$$

$$\gamma_{\rm loss} = \gamma^0_{\rm loss} - \gamma_p, \tag{55}$$

and

$$\gamma_{\rm gain} = \gamma^0_{\rm gain} - \gamma_p \tag{56}$$

with

$$\gamma^0_{\rm loss} = \Lambda_0(1+n_B) - {\rm Im}\left[\chi_2 + \frac{\lambda_2}{2}\right], \tag{57}$$

$$\gamma^0_{\rm gain} = \Lambda_0 n_B + {\rm Im}\left[\chi_2 - \frac{\lambda_2}{2}\right], \tag{58}$$

and $\gamma_p > 0$ by definition.

We now comment on the physical effect of the components (52)–(58). As found previously [23,30–33,39,74], the cavity frequency shift $\Delta\omega_0$ is directly set by the real part of χ_2. A comparison between Eqs. (19) and (49) indicates that the cavity intrinsic linewidth Λ_0 is also shifted by $\Delta\Lambda_0 = -2\,{\rm Im}[\chi_2]$. The dissipative processes with rates $\gamma_{\rm loss}$ and $\gamma_{\rm gain}$ correspond to standard single-photon emission and absorption which are widely considered in circuit QED. One can see from Eqs. (55)–(58) that ${\rm Im}[\chi_2]$ contributes to the asymmetry between the photon loss and gain rates $\gamma_{\rm loss}$ and $\gamma_{\rm gain}$ whereas ${\rm Im}[\lambda_2]$ contributes equally to $\gamma_{\rm loss}$ and $\gamma_{\rm gain}$. The coefficients ρ_p and γ_p account for the effect of the ac drive since they are nonzero only for $\beta_p \neq 0$. From Eq. (53), U_{cl} generates the two-photon coherent drive in ρ_p of Eq. (47). Such a term can be obtained with a degenerate parametric amplifier (see, for instance, Sec. 5.1.1 of Ref. [41]). It was also obtained in Ref. [6] by using a complex configuration with two microwave cavities coupled nonlinearly and subject to two off-resonant drives. Finally, the dissipative process with a rate γ_p generated by U_q is less usual. Its jump operator $L_p = \hat{a} + e^{i\varphi_p}e^{-i2\omega_0 t}\hat{a}^\dagger$ corresponds to a time-dependent coherent superposition of photon absorption and emission operators. From Eqs. (55) and (56), one could believe that γ_p decreases the single-photon loss and gain rates, but this is not effective because the rates γ_+ and γ_- through which $\gamma_{\rm loss}$ and $\gamma_{\rm gain}$ occur in the cavity action do not depend on γ_p. Indeed, from Eqs. (50), (51), (55), and (56), one has $\gamma_- = \gamma^0_{\rm loss} - \gamma^0_{\rm gain}$ and $\gamma_+ = \gamma^0_{\rm loss} + \gamma^0_{\rm gain}$. There remains a term in γ_p which occurs through the second and third lines of Eq. (49) on the same footing as ρ_p. We will illustrate the effect of this peculiar term in Sec. IV D 2 for the case of a double quantum dot and check that it corresponds to a "squeezing dissipation." In fact, such an effect can also be obtained by using a broadband squeezed bath input [43] or a cavity damping modulation [42]. It leads to the relaxation of the cavity to a squeezed state. In these references, squeezing superoperators are used to describe this effect, instead of the jump operator L_p, but one can check that there is a formal equivalence between the two descriptions [75]. Importantly, in our work, we have used a range of γ_p such that one has $\gamma_{\rm loss} > 0$ and $\gamma_{\rm gain} > 0$, as required by the definition of the Lindblad Eq. (46). When the drive amplitude β_p becomes so large that $\gamma_{\rm loss} < 0$ and/or $\gamma_{\rm gain} < 0$, we expect that higher order terms in β_p become relevant, which introduces new terms in the cavity action which are not necessarily Markovian. In this case, the Lindblad Eq. (46) is not relevant anymore. This limit is beyond the scope of this article.

2. *Cavity effective Lindblad equation to fourth order in g*

We now investigate the possibility to identify the path-integral approach of Sec. III with a Lindblad description up to fourth order in g. We expect an extra contribution

$$H^{\rm eff,4}_{\rm cav} = K\hat{a}^{\dagger 2}\hat{a}^2 \tag{59}$$

to the effective Hamiltonian (47), which corresponds to a Kerr photonic interaction. We also expect dissipative processes with rates and jump operators $(\gamma_j, \hat{L}_j) \in \mathcal{P}_4$ with

$$\mathcal{P}_4 = \{(K_{\rm loss}, \hat{a}^2), (K_{\rm gain}, \hat{a}^{\dagger 2}), (D, \hat{a}^\dagger\hat{a})\}. \tag{60}$$

The three processes in the above ensemble correspond respectively to two-photon loss, two-photon gain, and pure dephasing. This leads to an action contribution (see Appendix A)

$$S^{(4)}_{\rm Mark} = -\int_t [\bar{\varphi}_{cl}\bar{\varphi}_{cl} \quad \bar{\varphi}_{cl}\bar{\varphi}_q \quad \bar{\varphi}_q\bar{\varphi}_q]\cdot\mathcal{A}_M\cdot\begin{bmatrix}\varphi_{cl}\varphi_{cl}\\ \varphi_{cl}\varphi_q\\ \varphi_q\varphi_q\end{bmatrix} \tag{61}$$

with

$$\mathcal{A}_M = \begin{bmatrix} 0 & i\frac{K_-}{2} + K & -\frac{iD}{2} \\ -i\frac{K_-}{2} + K & -i(D+2K_+) & -i\frac{K_-}{2} + K \\ -\frac{iD}{2} & i\frac{K_-}{2} + K & 0 \end{bmatrix} \tag{62}$$

and $K_- = K_{\rm loss} - K_{\rm gain}$, $K_+ = K_{\rm loss} + K_{\rm gain}$. To establish a mapping with the path-integral description, we now have to compare the above matrix $\mathcal{A}_M$ with the matrix $\mathcal{A}$ of Eq. (39), which occurs in the effective action of the mesoscopic QED device to fourth order in g. Strikingly, $\mathcal{A}_M$ and $\mathcal{A}$ cannot be mapped in all situations. This is possible when the condition

$$\mathcal{C}_{Ldb} = \{(W_4 = 0) \text{ and } ({\rm Re}[U_4] = 0) \text{ and } (V_4 = \chi_4^*)\} \tag{63}$$

is fulfilled. Equation (63) represents a sufficient condition to have a description of the cavity dynamics in terms of a Lindblad equation to fourth order in g. For a given mesoscopic circuit, one can test this condition by evaluating numerically the different fourth-order mesoscopic correlators. When condition (63) is valid, one has

$$K = {\rm Re}[\chi_4], \tag{64}$$

$$K_{\rm loss/gain} = \mp{\rm Im}[\chi_4] + \frac{{\rm Im}[U_4]}{2} - \frac{{\rm Im}[\lambda_4]}{4}, \tag{65}$$

and

$$D = -2\,\mathrm{Im}[U_4]. \tag{66}$$

Hence, $\mathrm{Re}[\chi_4]$ generates the effective Kerr interaction (59). Remarkably, there exists an analogy between the expressions of the rates for the single- and two-photon stochastic processes, Eqs. (65) and Eqs. (57) and (58). Indeed, $\mathrm{Im}[\chi_4]$ provides an opposite contribution to two-photon loss and gain, like $\mathrm{Im}[\chi_2]$ does for single-photon processes. In contrast, $\mathrm{Im}[\lambda_4] - 2\,\mathrm{Im}[U_4]$ provides the same contribution to two-photon loss and gain, like $\mathrm{Im}[\lambda_2]$ does for single-photon processes. The term in $\mathrm{Im}[U_4]$ also contributes to photonic dephasing (term in D). This last effect does not have any analog to second order in g.

We could not find other contributions to the Hamiltonian (59) and the jump operator ensemble $\mathcal{P}_4$ of Eq. (60) to extend the mapping between the path-integral approach and the Lindblad description beyond the regime of validity of Eq. (63). It would be interesting to find a systematic method to derive a cavity evolution equation from the cavity action, in order to establish the necessary conditions for having the Lindblad description**.** Importantly, to fourth order in g, a systematic mapping cannot be expected since the dynamics of the cavity is not necessarily Markovian. For instance, there can be "memory" effects due to a coherent exchange of energy between the cavity and the mesoscopic circuit. This will be illustrated in the case of a noninteracting double quantum dot in Sec. IV E.

3. Summary: Total photonic Lindblad equation up to fourth order in g in the interaction picture

In practice, it is convenient to study the cavity dynamics in an interaction picture by considering the time evolution of the cavity density operator $\rho^I_{\mathrm{cav}}(t) = e^{i\omega_0\hat{a}^\dagger\hat{a}t}\rho_{\mathrm{cav}}(t)e^{-i\omega_0\hat{a}^\dagger\hat{a}t}$. In this picture, Eqs. (46)–(48), (59), and (60) lead to

$$\frac{\partial\rho^I_{\mathrm{cav}}(t)}{\partial t} = -i\big[H^{\mathrm{eff},I}_{\mathrm{cav}}, \rho^I_{\mathrm{cav}}\big] + \sum_j \gamma_j \mathcal{D}_{\hat{L}_j}\big(\rho^I_{\mathrm{cav}}\big) \tag{67}$$

with

$$H^{\mathrm{eff},I}_{\mathrm{cav}} = \Delta\omega_0\hat{a}^\dagger_I\hat{a}_I + i\rho_p\hat{a}^{\dagger 2}_I - i\rho^*_p\hat{a}^2_I + K\hat{a}^{\dagger 2}_I\hat{a}^2_I \tag{68}$$

and dissipative processes $(\gamma_j, \hat{L}_j) \in \mathcal{P}_I$ with

$$\mathcal{P}_I = \big\{(\gamma_{\mathrm{loss}}, \hat{a}_I), (\gamma_{\mathrm{gain}}, \hat{a}^\dagger_I), (\gamma_p, \hat{a}_I + e^{i\varphi_p}\hat{a}^\dagger_I), \big(K_{\mathrm{loss}}, \hat{a}^2_I\big), \big(K_{\mathrm{gain}}, \hat{a}^{\dagger 2}_I\big), (D, \hat{a}^\dagger_I\hat{a}_I)\big\} \tag{69}$$

with $\hat{a}_I = e^{-i\omega_0 t}\hat{a}$.

Interestingly, Eq. (67) appears as a generalization to fourth order in g of Eq. (12) obtained with the direct density matrix approach. Indeed, one can check that these two equations agree to second order in g, provided the assumption $\Lambda_0 = 0$ of Sec. II B is used. For this purpose, one must use the equalities

$$\chi_2 = \chi_B(\omega_0) - \chi_A(\omega_0) \tag{70}$$

and

$$\lambda_2|_{\omega_0\neq 0} = 2i\,\mathrm{Im}[\chi_A(\omega_0) + \chi_B(\omega_0)], \tag{71}$$

which are derived in Appendix D.

IV. THE CASE OF A DOUBLE QUANTUM DOT IN A CAVITY

A. Circuit description

We now apply the results of Sec. III to the case of a spin-degenerate double quantum dot coupled to a microwave cavity, represented schematically in Figs. 1(a) and 1(b). This circuit encloses two quantum dots L and R with a tunnel coupling t_{LR} such that $\hat{H}_{\mathrm{meso}}$ includes a term $t_{LR}\hat{c}^\dagger_L\hat{c}_R + t^*_{LR}\hat{c}^\dagger_R\hat{c}_L$. The dot $L(R)$ is contacted to a normal metal reservoir with a tunnel rate $\Gamma_{L(R)}$. Equation (1) gives $\Gamma_d = 2\pi\,\Sigma_{k\in C}|t_{k,d}|^2$ for $d \in L(R)$. The rate Γ_d can be considered as energy independent in the framework of a wide-band approximation for the reservoirs with $|t_{k,d}|^2$ independent of k. In the following, we consider the case $\Gamma_L = \Gamma_R = \Gamma$. A bias voltage V is applied between the two normal metal contacts. The orbital energy $\omega_{L(R)}$ of dot $L(R)$ can be finely tuned with an electrostatic gate. In principle, $\omega_{L(R)}$ can also be shifted by a fraction of eV, which depends on the ratio of the junctions capacitances. Here we will assume that this shift is negligible [76]. We will also disregard Coulomb interactions in the double dot. This basic case presents essential ingredients of mesoscopic QED: The cavity electric field can couple to both the internal transition between the L and R orbitals of the double dot and to tunnel transitions between the dots and the continuum of states of the normal metal reservoirs.

B. Unperturbed mesoscopic Green's function of the double dot

The unperturbed mesoscopic circuit Green's function $\check{G}$ of the double dot, whose inverse appears in Eq. (21), must be calculated in the absence of light/matter coupling (i.e., $g_L = 0$ and $g_R = 0$). It can be obtained by performing the inversion

$$\check{G}(\omega) = \begin{bmatrix} \tilde{G}^{-1}_r(\omega) & \tilde{M}_K \\ \tilde{0} & \tilde{G}^{-1}_a(\omega) \end{bmatrix}^{-1} \tag{72}$$

with [77,78]

$$\tilde{G}^{-1}_{r(a)}(\omega) = \begin{bmatrix} \omega - \omega_L \pm i\frac{\Gamma}{2} & -t_{LR} \\ -t^*_{LR} & \omega - \omega_R \pm i\frac{\Gamma}{2} \end{bmatrix} \tag{73}$$

and

$$\tilde{M}_K = \begin{bmatrix} i\Gamma(1 - 2n_{F,L}(\omega)) & 0 \\ 0 & i\Gamma(1 - 2n_{F,R}(\omega)) \end{bmatrix}. \tag{74}$$

Equations (73) and (74) stem from the explicit definitions (24)–(26) of the Green's functions $\tilde{G}_{r/a/K}(\omega)$ in terms of fermionic operators and the expression of the double dot circuit Hamiltonian [see Eq. (2) with $g_{L(R)} = 0$]. Since we consider a spin-degenerate situation with noninteracting quantum dots, the spin degree of freedom is omitted in the above orbital subspace structure. We will restore it later in numerical evaluations by taking into account an implicit multiplication by a factor 2 in the traces operator over the orbital index d. The Fermi occupation function $n_{F,L(R)}(\omega) = \{1 + \exp[(\omega \mp (eV_b/2))/k_BT]\}^{-1}$ of the $L(R)$ contact is affected by the bias voltage V_b. For later use, we also define the lesser self-energy of the double dot [77]

$$\tilde{\Sigma}^<(\omega) = \begin{bmatrix} i\Gamma n_{F,L}(\omega) & 0 \\ 0 & i\Gamma n_{F,R}(\omega) \end{bmatrix} \tag{75}$$

and the light/matter coupling matrix

$$\check{g} = \mathrm{diag}[g_L, g_R, g_L, g_R]. \tag{76}$$

C. Choice of parameters

For simplicity, we will use a nonzero g_L and $g_R = 0$, which corresponds to DQD experiments realized so far, where a very asymmetric microwave coupling to the two dots is engineered. In experiments realized with standard coplanar microwave resonators, the light matter coupling is typically $g_L \approx 0.001\omega_0$ [18]. In a more recent design based on high kinetic inductance superconducting nanowire resonators, $g_L \approx 0.03\omega_0$ was reached [28]. However, since the rms voltage of these resonators is [79] $V_{rms} = 20\ \mu V \simeq 4.9$ GHz for $\omega_0 \approx 4$ GHz, one can reach $g_L \sim \omega_0$, in principle, by using a galvanic coupling between one of the dots and the cavity. In this work, we consider the regime $\Lambda_0 \ll \Gamma$ explored experimentally, with $\Gamma \geqslant 0.005\omega_0$. We also use $g_L/\omega_0 \leqslant 0.125$ and $\beta_p g_L^3/\omega_0^3 \leqslant 0.001$.

Since we develop the cavity action with respect to g_L and β_p, the amplitude of these two parameters must not be too large. Besides, having $\Gamma \neq 0$ is crucial for ensuring the validity of our perturbation scheme. Indeed, in the absence of dissipation, the correlators χ_2 and χ_4 are expected to diverge at $\omega_{\mathrm{DQD}} = \omega_0$ and/or $\omega_{\mathrm{DQD}} = 2\omega_0$ [80]. However, giving a simple analytic criterion for the regime of validity of our development is very complex because of the many parameters involved in the problem and because these parameters occur in the system description through complicated functional dependences (see the expressions of χ_2, λ_2, U_{cl}, U_q, χ_4, λ_4, U_4, V_4, and W_4). Alternatively, one can check that the next-order mesoscopic correlators in g^6 and g^8 are negligible. This is discussed in detail in Appendix H. We have checked that we remain on the safe side with the parameters used in the present work.

D. The low coupling limit: Squeezed photonic vacuum induced by a double quantum dot

1. Evaluation of the Lindblad equation coefficients to third order in g_L

We have seen above that U_{cl} corresponds to a coherent two-photon drive whereas U_q corresponds to an unusual form of squeezing dissipation. In this section, we evaluate these coefficients in the double dot case. Figure 3 shows $|U_{cl}|$ and $|U_q|$ versus the dot orbital energies ω_L and ω_R, for moderate tunnel rates $\Gamma = 0.1\omega_0$ and a moderate interdot hopping $t_{LR} = 0.1\omega_0$. We use a zero bias voltage in Figs. 3(a) and 3(b) and a nonzero bias voltage $V_b = 1.5\omega_0$ in Figs. 3(c) and 3(d). Both U_{cl} and U_q show strong resonances which appear as diagonal lines in Fig. 3. These lines correspond to resonances of the cavity with the double dot internal degree of freedom [see Fig. 3(e)]. More precisely, the bonding and antibonding states of the double dot, which result from the tunnel coupling between the left and right orbitals, have energies $\omega_{\mp} = (\omega_L + \omega_R \mp \sqrt{\Delta\omega_{LR}^2 + 4t_{LR}^2})/2$ with $\Delta\omega_{LR} = \omega_L - \omega_R$ being the dots' orbital detuning. In principle, single-photon resonances $\omega_{\mathrm{DQD}} = \omega_0$, with $\omega_{\mathrm{DQD}} = \omega_+ - \omega_-$ by definition, are expected for $\Delta\omega_{LR} = \pm R(\omega_0)$ with $R(\omega_0) = \sqrt{\omega_0^2 - 4t_{LR}^2}$,

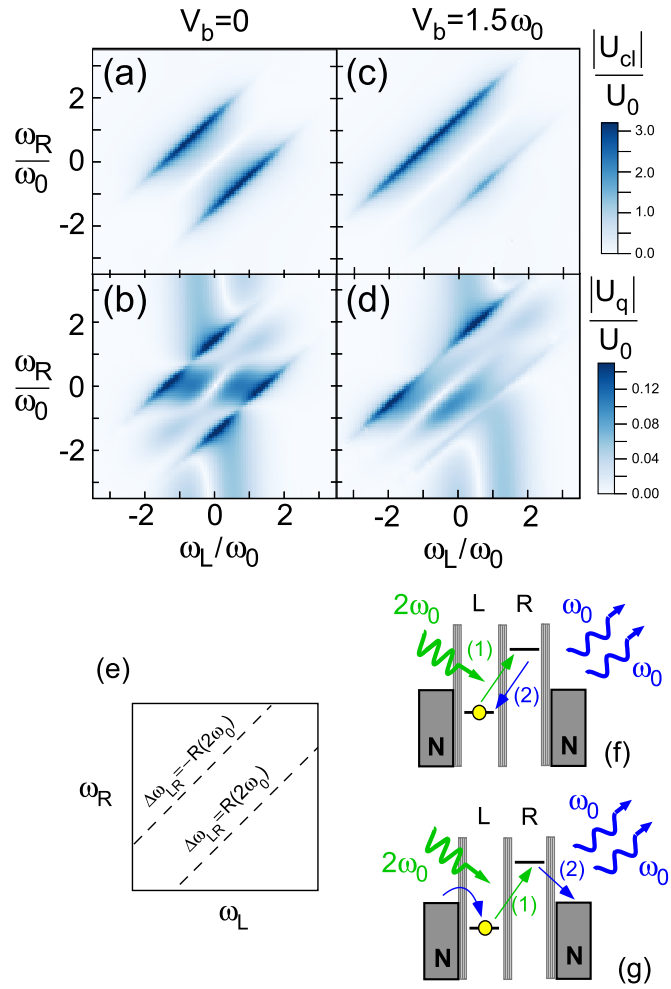

FIG. 3. [(a)–(d)] Absolute values of the coefficients U_{cl} and U_q which account for the effect of the $2\omega_0$ drive of the cavity at order 3 in the photon/dot coupling g_L, vs the dot orbital energies ω_L and ω_R. Panels (a) and (b) correspond to a bias voltage $V_b = 0$ and panels (c) and (d) to $eV_b = 1.5\omega_0$. The other parameters are $\Gamma = 0.1\omega_0$, $t_{LR} = 0.7\omega_0$, $k_BT = 0.275\omega_0$, $g_R = 0$, and $\Lambda_0 = 5.10^{-5}\omega_0$. We use a normalization factor $U_0 = g_L^3\beta_p/\omega_0^2$. Panel (e) indicates the positions of the two-photon resonances $\omega_{\mathrm{DQD}} = 2\omega_0$ between the dot internal degree of freedom and the cavity, which are obtained for $\Delta\omega_{LR} \simeq \pm R(2\omega_0)$. [(f), (g)] Examples of coherent and dissipative processes in g_L^3 involving the $2\omega_0$ drive, for $\Delta\omega_{LR} \simeq \pm R(2\omega_0)$. When the internal transition of the double dot matches $2\omega_0$, it can absorb a $2\omega_0$ photon. This enables the emission of two ω_0 photons upon electronic transitions which are internal to the dot (f) or involve the normal metal contacts (g).

and two-photon resonances $\omega_{\mathrm{DQD}} = 2\omega_0$ are expected for $\Delta\omega_{LR} = \pm R(2\omega_0)$. In Fig. 3, only the two-photon resonances are visible because we use $2t_{LR} > \omega_0$ and therefore the condition $\Delta\omega_{LR} = \pm R(\omega_0)$ can never be satisfied. Figs. 3(f) and 3(g) show some examples of two-photon processes which are expected to contribute to the resonances at $\Delta\omega_{LR} = \pm R(2\omega_0)$. A photon with frequency $2\omega_0$ can be converted into two photons with frequency ω_0, in tunneling sequences which can be either purely coherent [Fig. 3(f)] or dissipative [Fig. 3(f)]. Interestingly, the gate voltage area where the two-photon resonances appear is modified when a nonzero bias voltage is used

[Figs. 3(c) and 3(d)]. This is because the third-order processes such as the one shown in Figs. 3(f) and 3(g) require that the double dot bonding and antibonding states are occupied and empty respectively, and the transport processes induced by a nonzero V_b modify the occupation of these states. Therefore, using a nonzero bias voltage can be useful to trigger two-photon processes, especially in case of weak tunability of $\omega_{L(R)}$, which can happen for some types of quantum dots. Interestingly, $|U_q|$ also shows broad vertical resonances (for ω_L constant) outside of the gap between the $\Delta\omega_{LR} = R(2\omega_0)$ and $\Delta\omega_{LR} = -R(2\omega_0)$ resonances [see Figs. 3(b) and 3(d)]. These resonances are due to tunneling between the left dot and the left reservoir, due to the conditions $g_L \neq 0$ and $\Gamma \neq 0$. As expected, these resonances shift with V_b [compare Figs. 3(b) and 3(d)] and get thinner when Γ decreases (not shown). The transition between the right reservoir and the right dot is not directly coupled to the cavity since $g_R = 0$, but a broad horizontal resonance also appears in Fig. 3(b) between the lines $\Delta\omega_{LR} = R(2\omega_0)$ and $\Delta\omega_{LR} = -R(2\omega_0)$ because the hybridization between the left and right orbitals enables tunneling to the right reservoir. Note that the horizontal and vertical resonances induced by the presence of the normal metal reservoirs are visible in $|U_q|$ but not in $|U_{cl}|$. This can be explained by the fact that tunneling to the normal metal reservoirs is a stochastic effect which impacts more directly the dissipative processes in γ_p (or U_q) than the coherent drive in ρ_p generated by U_{cl}.

2. Stationary Wigner function of the cavity to third order in g_L

To characterize the effects of the terms in U_{cl} and U_q, we now calculate analytically the stationary cavity Wigner function which follows from Eq. (67) to third order in g, i.e., assuming that the terms in K, K_{loss}, K_{gain}, and D are negligible. The cavity Wigner function can be defined quite generally as

$$W(\alpha,\alpha^*,t) = \frac{1}{\pi^2}\int d^2\beta e^{(\beta^*\alpha-\alpha^*\beta)}\langle e^{\beta\hat{a}_I^\dagger-\beta_I^*\hat{a}_I}\rangle_t. \tag{77}$$

Following the method of Ref. [41], one can show that Eq. (67) leads to the evolution equation

$$\begin{aligned}\frac{\partial}{\partial t}W =& \left(-i\Delta\omega_0\left[\frac{\partial}{\partial\alpha^*}\alpha^* - \frac{\partial}{\partial\alpha}\alpha\right]\right)W \\ &+ \left[\frac{\gamma_+}{2}\frac{\partial}{\partial\alpha}\frac{\partial}{\partial\alpha^*} + \frac{\gamma_-}{2}\left(\frac{\partial}{\partial\alpha}\alpha + \frac{\partial}{\partial\alpha^*}\alpha^*\right)\right]W \\ &- \left(2\rho_p\frac{\partial}{\partial\alpha}\alpha^* + 2\rho_p^*\frac{\partial}{\partial\alpha^*}\alpha\right)W \\ &- \gamma_p\left(\frac{e^{-i\varphi_p}}{2}\frac{\partial^2}{\partial\alpha^{*2}} + \frac{e^{i\varphi_p}}{2}\frac{\partial^2}{\partial\alpha^2}\right)W\end{aligned} \tag{78}$$

(see details in Appendix E). The term in γ_p in Eq. (78) describes a squeezing dissipation similar to Refs. [42,43]. In the stationary regime, the solution of this equation is

$$W(\alpha,\alpha^*,t\to+\infty) = \frac{1}{\pi\sqrt{A^2-4|B|^2}}\exp\left(\frac{P}{A^2-4|B|^2}\right) \tag{79}$$

with

$$P = A|\alpha|^2 + B^*\alpha^2 + B\alpha^{*2} \tag{80}$$

and, to third order in g and first order in ε_p,

$$A = -\gamma_+/2\gamma_- \tag{81}$$

and

$$B = \left(\rho_p\frac{\gamma_+}{\gamma_-} - \gamma_p\frac{e^{i\varphi_p}}{2}\right)\Big/(\gamma_- + 2i\Delta\omega_0). \tag{82}$$

Equation (79) describes a squeezed cavity vacuum. The major axis of the squeezed Gaussian is tilted by an angle $\theta = \arg[B]/2$ from the $\text{Re}[\alpha]$ axis. The fields quadratures along the θ and $\theta+\pi/2$ angles have the variances $\Delta X_\pm = \sqrt{-(A/2)\pm|B|}$. Strinkingly, from Eq. (82), the coherent drive in ρ_p and the dissipation processes in γ_p can both contribute to cavity squeezing and interfere constructively or destructively depending on the value of the phase φ_p. Note that expression (79) is valid for any type of mesoscopic circuit with internal degrees of freedom coupled to the cavity electric field, as long as (67) can be treated to third order in g. In Appendix F, we study in more detail the influence of the double dot parameters on the photonic squeezing. Note that squeezing has already been found in various mesoscopic QED configurations [44–46].

E. Photonic Schrödinger cat states produced by a double quantum dot

Obtaining Schrödinger cat states is useful to study the quantum behavior of a device on a fundamental level as well as to develop quantum computers. To obtain such states with our device, we need to invoke the fourth-order terms in g_L of Eqs. (59) or (60), which will generate multistability in the cavity behavior. For simplicity, we will perform the study of this situation in the particular case where the system dynamics can be described by a Lindblad equation. This limit presents the advantage of remaining formally simple while demonstrating interesting potentialities of mesoscopic QED.

1. Double dot correlation functions to fourth order in g_L

In the double dot case, can the Lindblad description hold to fourth order in g_L, or equivalently, can the condition $\mathcal{C}_{Ldb}$ of Eq. (63) be satisfied? To answer this question, we show in Fig. 4 the dependence of the coefficients χ_4, λ_4, U_4, V_4, and W_4 on $\Delta\omega_{LR}$, for a zero bias voltage ($V_b = 0$) and low tunnel rates ($\Gamma = 0.01\omega_0$). Figures 4(a) and 4(c) show that $\mathcal{C}_{Ldb}$ is not true when the double dot is resonant with the cavity [$\omega_{\text{DQD}} = \omega_0$, i.e., $\Delta\omega_{LR} \sim R(\omega_0)$]. This is not surprising, because, in this case, real energy exchanges between the double dot and the cavity are possible, leading to vacuum Rabi oscillations in the case of low Γ and Λ_0. Hence, for the cavity, the mesoscopic circuit represents a "bath with memory," which is incompatible with an effective Markovian dynamics. Another interesting regime is $\omega_{\text{DQD}} = 2\omega_0$, i.e., $\Delta\omega_{LR} \sim \pm R(2\omega_0)$, because the electronic correlation functions in g_L^4 present resonances in this area, as already seen for U_{cl} and U_q to third order in g_L. The Lindblad condition (63) is satisfied for $\Delta\omega_{LR} \sim \pm R(2\omega_0)$ with small values of Γ and t_{LR}, and $V_b = 0$ [see Figs. 4(b) and 3(d)] as well as a nonzero

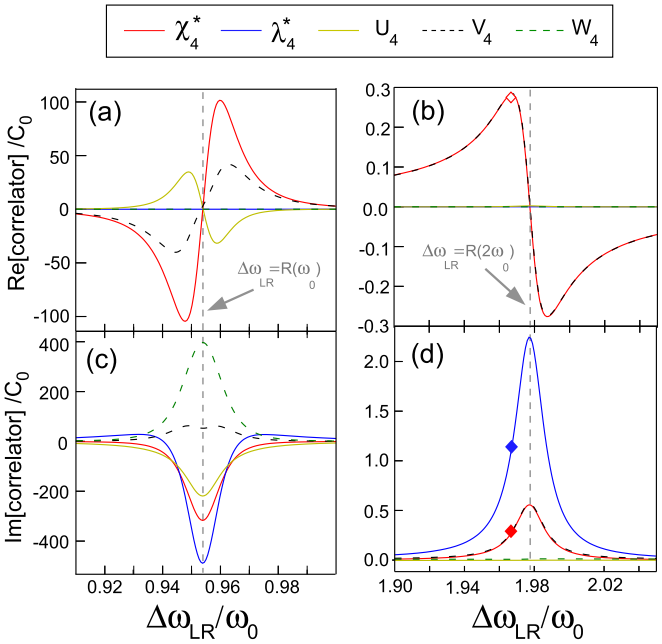

FIG. 4. Fourth-order electronic correlation functions vs $\Delta\omega_{LR}$ calculated for $\omega_{av} = (\omega_L + \omega_R)/2 = 0.989\omega_0$, $\Gamma = 0.01\omega_0$, $t_{LR} = 0.15\omega_0$, $k_BT = 0.3\omega_0$, $eV_b = 0$, $g_R = 0$, $\beta_p = 0.35$, and $\Lambda_0 = 10^{-4}\omega_0$. Panels (a) and (b) show the real parts of the correlators and panels (c) and (d) show the imaginary parts. The left panels show the area $\Delta\omega_{LR} \sim R(\omega_0)$ (which implies $\omega_{\rm DQD} \sim \omega_0$) whereas the right panels show $\Delta\omega_{LR} \sim R(2\omega_0)$ (which implies $\omega_{\rm DQD} \sim 2\omega_0$). All correlation functions are normalized by $C_0 = g_L^4/\omega_0^3$. The full and empty diamonds correspond to reference points for a comparison with Fig. 5. The mapping condition (63) is satisfied when the red full lines and black dashed lines coincide in the top and bottom panels ($\chi_4^* = V_4$), the green dashed line is close to 0 in both panels ($W_4 = 0$), and the yellow line is close to zero in the top panel ($\mathrm{Re}[U_4] = 0$). This is true for panels (b) and (d).

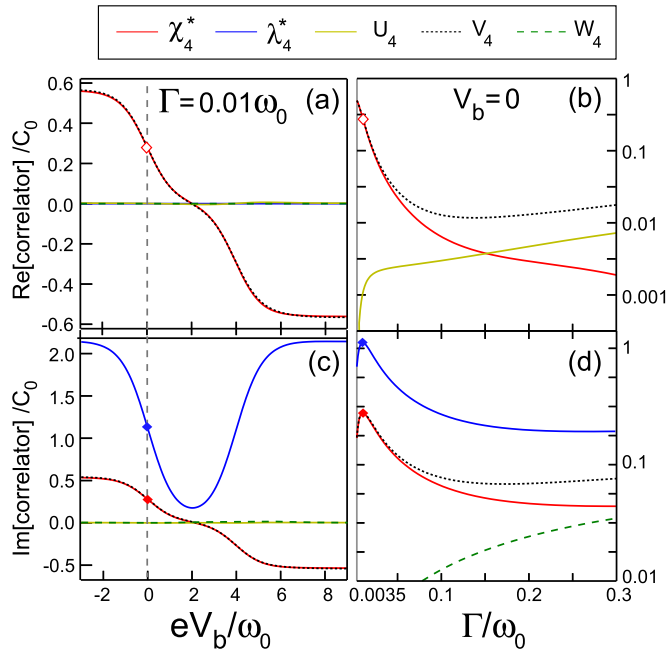

FIG. 5. Fourth-order electronic correlation functions vs V_b for $\Gamma = 0.01\omega_0$ [(a), (c)] and vs Γ for $V_b = 0$ [(b), (d)]. We use $\omega_{av} = 0.989\omega_0$ and $\Delta\omega_{LR} = 1.967\omega_0$. The other parameters are the same as in Fig. 4. The diamonds correspond to reference points identical to those of Fig. 4.

V_b [see Figs. 5(a) and 5(b)]. More generally, the Lindblad condition $\mathcal{C}_{Ldb}$ is satisfied when the cavity and double dot are off-resonant (for single-photon exchange) and the dot-lead and dot-dot couplings weak enough ($\Gamma, t \ll \omega_0 - \omega_{\rm DQD}$).

One may attribute this result to the fact that, in this regime, there can only be virtual energy exchanges between the cavity and the double dot, which occur on a timescale which is very short in comparison with the typical timescale for the evolution of the cavity. The condition $\mathcal{C}_{Ldb}$ is not valid anymore for higher tunnel rates $\Gamma > 0.1\omega_0$ [see Figs. 5(b) and 5(d)]. Indeed, in this case the resonances at $\Delta\omega_{LR} \sim R(\omega_0)$ and $\Delta\omega_{LR} \sim R(2\omega_0)$ start overlapping and the distinction between real and virtual energy exchanges between the cavity and the double dot becomes less clear. The condition $\mathcal{C}_{Ldb}$ is not valid either for $\Delta\omega_{LR} \sim R(2\omega_0)$ and t_{LR} large ($t_{LR} > 0.3\omega_0$) (not shown). This is why, in the rest of this section, we will focus on the Lindbladian dynamics of the cavity for $\Delta\omega_{LR} \sim R(2\omega_0)$, $t_{LR} \lesssim 0.15\omega_0$, and $\Gamma \lesssim 0.1\omega_0$. Note that for $\Gamma \to 0$, the imaginary part of the electronic correlators vanishes [see the very left of Fig. 5(d) for the onset of this effect]. Since we are interested in the effect of a genuinely dissipative mesoscopic circuit, we will only consider the case $\Gamma \geqslant 0.005\omega_0$ in the following. In particular, we will consider the working point $\Gamma \simeq 0.01\omega_0$ where $|\mathrm{Im}[\chi_4]|$ and $|\mathrm{Im}[\lambda_4]|$ have a local maximum [see very left of Fig. 5(d)]. Figure 6 represents some possible photonic processes at fourth order in g_L in this limit [see Figs. 6(a), 6(b$_1$), 6(b$_2$), 6(b$_3$), and 6(c)], for different configurations of dot orbital energies and bias voltage. It also shows $K_{\rm loss}$ and $K_{\rm gain}$ versus $\Delta\omega_{LR}$ and V_b for the parameters of Figs. 4 and 5 with $\Gamma = 0.01\omega_0$ and $\Delta\omega_{LR} = R(2\omega_0)$. In these conditions, one can check that for $V_b = 0$, the two-photon stochastic dissipation rate $K_{\rm loss}$ is the dominant stochastic rate in Eq. (69), i.e., $K_{\rm gain}$, D, $\gamma_{\rm loss}$, and $\gamma_{\rm gain}$ are much weaker. The rate $K_{\rm loss}$ corresponds to the type of processes represented in Figs. 6(b$_1$) and 6(b$_2$), where two photons can be absorbed simultaneously by the double dot circuit because the double dot is resonant with $2\omega_0$, and this absorption is made irreversible by the presence of the normal metal reservoirs. The working point $\omega_{av} = 0$ and $\Delta\omega_{LR} = R(2\omega_0)$ corresponds to a maximal $K_{\rm loss}$ for $V_b = 0$ [see Fig. 6(b$_2$)]. For comparison, in the configuration of Fig. 6(b$_1$), $K_{\rm loss}$ is weaker because the filling of the lower dot level is less efficient. Remarkably, a nonzero V_b can be used to obtain a nonzero $K_{\rm gain}$ and change the relative values of $K_{\rm loss}$ and $K_{\rm gain}$ (see bottom right panel of Fig. 6). For $V_b < 0$, $K_{\rm loss}$ increases because the filling of the lower dot level and/or the emptying of the upper dot level by the normal metal reservoirs becomes more efficient and this enhances the "reset" of the double dot between two-photon pair absorption processes [Fig. 6(b$_3$)]. For $V_b > 0$ and sufficiently large, the filling of the upper dot level and emptying of the lower dot level are favored, which causes photon pair emission processes [see Fig. 6(c)] while $K_{\rm loss}$ vanishes. In this limit, the emission of photon pairs is obtained without any need

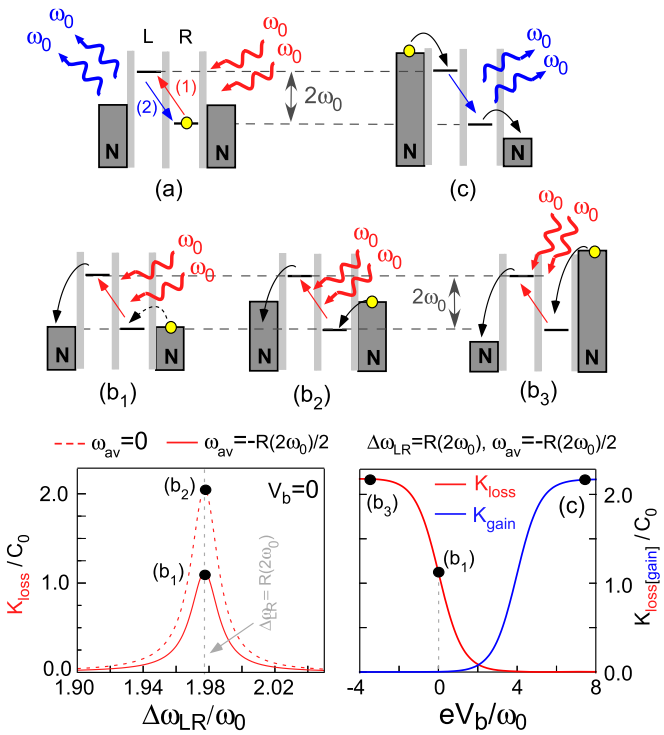

FIG. 6. Example of processes at fourth order in the light/matter coupling g_L. Panel (a) shows a fully coherent process which involves only the internal transition of the double dot and can contribute to the term in K. Panels (b_1), (b_2), and (b_3) show processes which involve irreversible tunneling to the normal metal reservoirs and contribute to $K_{\rm loss}$ for different configurations of dot orbital energies and bias voltage. Panel (c) shows a process which contributes to $K_{\rm gain}$ in the presence of a finite bias voltage. The left bottom plot shows $K_{\rm loss}$ vs ω_{LR} for two difference values of ω_{av}, i.e., $\omega_{av} = R(2\omega_0)/2$ (full red line) and $\omega_{av} = 0$ (dashed red line). The right bottom plot shows $K_{\rm loss}$ (red full line) and $K_{\rm gain}$ (blue full line) vs V_b for $\omega_{av} = R(2\omega_0)/2$. The same parameters as in Figs. 4 and 5 are used.

for an ac cavity excitation ($\varepsilon_p = 0$) because the mesoscopic bias in V_b provides the energy for this process. The Kerr interaction K, which corresponds to the processes of Fig. 6(a), varies like $\mathrm{Re}[\chi_4]$, which is represented in Figs. 4 and 5. Strikingly, for $V_b = 0$, K cancels at $\Delta\omega_{LR} = R(2\omega_0)$, where $K_{\rm loss}$ is maximal [see Figs. 4(b) and 4(b)]. Importantly, in all these plots, the order of magnitude of $K_{\rm loss}$, $K_{\rm gain}$, and K is given by the constant $C_0 = g_L^4/\omega_0^3$. Using the typical value $\omega_0 = 2\pi \times 5$ GHz and the ratio $g_L = 0.125$ which is strong but experimentally feasible, in principle (see Sec. IV C), one finds $C_0 = 2\pi \times 1.2$ MHz. We will see in next sections that this is sufficient to obtain sizable nonlinear signatures in the cavity response.

2. *Average photon number*

Before studying the full quantum behavior of the cavity through the Wigner function W, it is useful to study the mean value of $\langle \hat{a} \rangle$ which can be expressed analytically. This can reveal a multistable behavior which is expected for driven nonlinear systems [41] and which will be useful to obtain photonic Schrödinger cats. From the Lindblad Eq. (46) with the fourth-order terms (59) and (60) included and $\langle \hat{a} \rangle = \alpha_{av} e^{-i\omega_0 t}$, one gets

$$U_{cl}\alpha_{av}^* - \left(\frac{\Lambda_0 + \Delta\Lambda_{0,4}}{2} + i\chi_2 + 2i\chi_4|\alpha_{av}|^2\right)\alpha_{av} = 0 \quad (83)$$

with

$$\Delta\Lambda_{0,4} = \mathrm{Im}[\lambda_4 - 4(\chi_4 + U_4)] \quad (84)$$

being the renormalization of the cavity linewidth to fourth order in g_L. Equation (83) bears similarities with the result given by semiclassical approaches (see Appendix B), but the term $\Delta\Lambda_{0,4}$ is specific to a full quantum-mechanical treatment. The solution $\alpha_{av} = 0$ is obvious. However, in principle, Eq. (83) can also give nonzero values of $\alpha_{av} = \alpha_{av}^{\pm}$ given by

$$\alpha_{av}^{\pm} = \frac{1}{|\chi_4|}\sqrt{\frac{-\mathrm{Re}\left[\chi_2^{\rm ren}\chi_4^*\right] \pm \sqrt{\Delta}}{2}} \quad (85)$$

with

$$\Delta = |\chi_4|^2|U_{cl}|^2 - \mathrm{Im}\left[\chi_2^{\rm ren}\chi_4^*\right]^2 \quad (86)$$

and $\chi_2^{\rm ren} = \chi_2 - i(\Lambda_0 + \Delta\Lambda_{0,4})/2$. Importantly, α_{av} must be real. Hence, from Eq. (85) for low amplitudes of β_p, the only possible solution is $\alpha_{av} = 0$ since $\Delta < 0$. For a stronger drive ($|U_{cl}| > |\mathrm{Im}\,[\chi_2^{\rm ren}\chi_4^*]/\chi_4|$), Δ becomes positive. Then, the comparison between $\sqrt{\Delta}$ and $\pm\mathrm{Re}[\chi_4^*\chi_2^{\rm ren}]$ sets whether there are 0, 1, or 2 values of α_{av} allowed by Eq. (85). Finally, two values for α_{av} are possible for each value of φ_{av}, i.e.,

$$\varphi_{av}^{\pm} = -\frac{1}{2}\arg\left[\frac{i\chi_2^{\rm ren} + 2i\chi_4\alpha_{av}^{\pm 2}}{U_{cl}}\right] + n\pi \quad (87)$$

with $n \in \{0, 1\}$. In some cases, we find that α_{av}^+ and α_{av}^- can be both solutions to Eq. (83). However, for simplicity, we focus below on the situation of moderate interdot hopping ($t_{LR} = 0.15\omega_0$), moderate tunnel rates ($0.005\omega_0 \leqslant \Gamma \leqslant 0.1\omega_0$), and a zero bias voltage ($V_b = 0$), where one has typically a single nonzero solution α_{av}^+. In particular, for the parameters considered in Fig. 7, one has $|U_{cl}| \gg |U_q|$, $K = \mathrm{Re}[\chi_4] \ll -\mathrm{Im}[\chi_4]$, and $\mathrm{Im}[\chi_4] < 0$. Therefore, one has $\alpha_{av}^+ \simeq \alpha_{av,I}^+$ with

$$\alpha_{av,I}^+ = \sqrt{\frac{\mathrm{Im}\left[\chi_2^{\rm ren}\right] + \sqrt{|U_{cl}|^2 - \mathrm{Re}\left[\chi_2^{\rm ren}\right]^2}}{-2\,\mathrm{Im}[\chi_4]}}. \quad (88)$$

This quantity is represented with black crosses in Fig. 7 and is in excellent agreement with the exact α_{av}^+ represented with a cyan line. Equation (88) shows the crucial role of the two-photon dissipation provided by the term in $\mathrm{Im}[\chi_4]$ for the creation of nonzero photon states (if one had $|\chi_4| \to 0$, α_{av}^+ would diverge and thus become physically irrelevant). Of course, it is also necessary to have a high enough U_{cl}. A crude approximation is obtained by using $\chi_2^{\rm ren} = 0$, which yields

$$\alpha_{av,II}^+ = \sqrt{\frac{2|\rho_p|}{K_{\rm loss} - K_{\rm gain}}} \quad (89)$$

(see red crosses in Fig. 7). This expression shows well that the nonzero α_{av}^+ results from a balance between two-photon coherent injection and two-photon dissipation. In contrast, the effect of the Hamiltonian Kerr term K is negligible in Fig. 7. The comparison between $\alpha_{av,I}^+$ and $\alpha_{av,II}^+$ shows that the

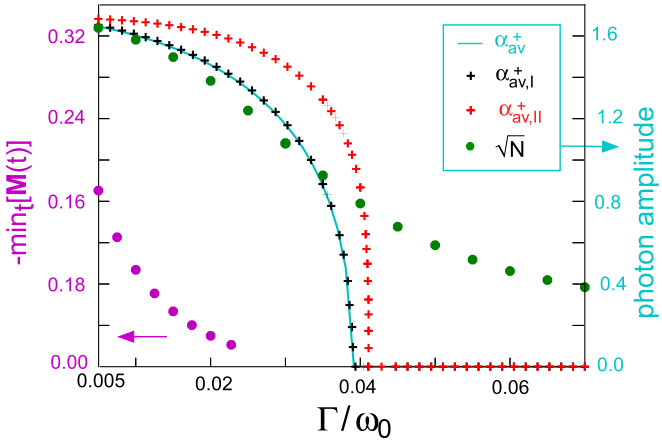

FIG. 7. Various characteristics of the cavity response vs the tunnel rate to the normal metal reservoirs Γ in the presence of the cavity drive in ε_p treated at fourth order in g_L. We use $\omega_{av} = 0.989\omega_0$, $g_L = 0.125\omega_0$, and $\Delta\omega_{LR} = R(2\omega_0) \simeq 1.978\omega_0$. The other parameters are the same as in Fig. 4. The full cyan line, the black crosses, and the red crosses show the semiclassical photon amplitudes α^+_{av} and its approximations $\alpha^+_{av,I}$ and $\alpha^+_{av,II}$ of Eqs. (85), (88), and (89), respectively. The green dots show the square root of the average photon number N in the cavity in stationary conditions, obtained from Eq. (67). The magenta dots show the maximum negativity of the Wigner function over time t and over the quadratures α, α^* for the protocol discussed in Sec. IV E 3 where the cavity drive is switched on suddenly.

single-photon processes described by $\chi_2^{\rm ren}$ slightly decrease the amplitude of α^+_{av} and the range of Γ for which cavity bistability is obtained. Note that, in principle, one has to study the stability of the $\alpha^\pm_{av}$ solutions to determine their relevance. We will omit such a study because the cavity Wigner function calculated in Sec. IV E 3 provides this information for the regime we are interested in.

3. Cavity Wigner function to fourth order in g_L in nonstationary conditions

So far, we have studied the cavity Wigner function W in stationary conditions. We now assume that the cavity is initially in the stationary vacuum state obtained in the absence of the microwave drive ($\beta_p = 0$). We want to study the time evolution of W when we switch on β_p at $t = 0$. However, since we have derived the terms in β_p in Eq. (67) in stationary conditions [see Eq. (3) and Appendix A], one has to be careful about the validity of this equation which could be jeopardized by the sudden rise of β_p. In fact, Eq. (67) will still be valid in the transient regime if we impose two constraints on the rise time of β_p. On the one hand, we will assume that this rise time is much longer that the correlation time $\sim 1/\Gamma$ associated to tunneling to the mesoscopic reservoirs, so that the terms U_{cl} and U_q in the cavity effective action can still be defined at any time from Eqs. (33) and (34) with a prefactor β_p which depends on t. On the other hand, we will assume that the rise time of β_p is much faster than the cavity characteristic evolution time [visible in Fig. 8(c)]. In these conditions, it is sufficient to use the Lindblad Eq. (67) with terms (59) and

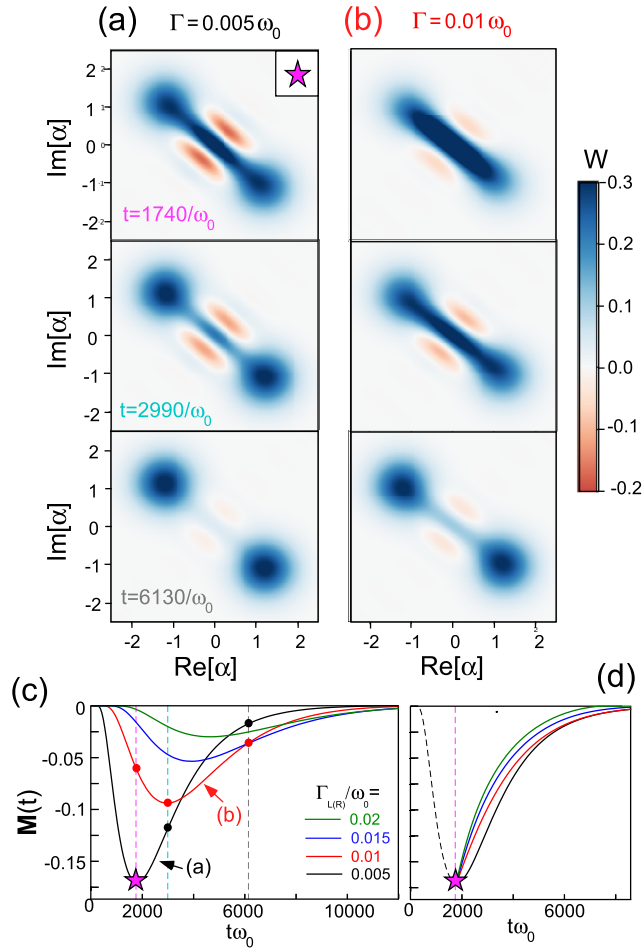

FIG. 8. [(a), (b)] Wigner function W of the cavity for tunnel rates $\Gamma = 0.005\omega_0$ and $\Gamma = 0.01\omega_0$ and different times t after switching on the cavity drive in ε_p ($t\omega_0 = 1740$, 2990, 6130 from top to bottom). The other parameters are the same as in Fig. 7. (c) Minimum $\mathbf{M}(t)$ of the Wigner function W over the field quadratures, vs t, for the same protocol as in panels (a) and (b), and different tunnel rates. The black and red curves correspond to panels (a) and (b) respectively. (d) Relaxation of $\mathbf{M}(t)$ vs time, starting from the initial state shown in panel (a) at $t = 1740/\omega_0$, for different values of Γ.

(60) which depend on $\beta_p(t) = \beta_p\theta(t)$ with $\theta(t)$ being the Heavidside function.

We compute $W(t)$ numerically by using the function "mesolve" from the qutip package to solve Eq. (67) [81]. For moderate tunnel rates, the cavity evolves toward a coherent superposition of two coherent states [see Figs. 8(a) and 8(b)]. The nonclassicality of $W(t)$ is revealed by the red areas where $W(t) < 0$. At large times, there remains only two positive spots in the Wigner function, which are approximately centered on the average values $\alpha^+_{av}e^{i\varphi^+_{av}}$ and $-\alpha^+_{av}e^{i\varphi^+_{av}}$ determined in Sec. IV E 2. Therefore, these two solutions represent cavity stable states in stationary conditions. Accordingly, we have checked that the square root $\sqrt{N}$ of the average number $N = \langle\hat{a}^\dagger\hat{a}\rangle$ of photons in the cavity calculated numerically for $t \to +\infty$ matches α^+_{av} when the tunnel rate Γ is small (see green dots in Fig. 7). For higher tunnel rates, this is not the case anymore because $\alpha^+_{av} = 0$ whereas $W(t)$ corresponds to a squeezed vacuum. From the case $\Gamma/\omega_0 = 0.005$ [Fig. 8(a)]

to the case $\Gamma/\omega_0 = 0.01$ [Fig. 8(b)], the semiclassical minima of the Wigner function $W(t)$ keep approximately the same position in the quadratures space, because $|\rho_p|$ and $K_{\rm loss}$ are both approximately divided by two, and because from Eq. (89) it is the ratio between $K_{\rm loss}$ and $|\rho_p|$ which roughly determines the value of $|\alpha_{av}|$ (one has $|\rho_p| = 7.710^{-4}\omega_0$ and $K_{\rm loss} = 5.410^{-4}\omega_0$ in the black case, and $|\rho_p| = 3.7\,10^{-4}\omega_0$, $K_{\rm loss} = 2.7\,10^{-4}\omega_0$ in the red case, and $K_{\rm gain}$ is negligible in both cases).

Figure 8(c) represents the time evolution of the minimum negativity $\mathbf{M}(t) = \min_{\alpha,\alpha^*}[W(t)]$ of the Wigner function $W(t)$ over the field quadratures (α, α^*). When Γ increases, the minimum of $\mathbf{M}(t)$ over time is reached later. This is because, from the black curve ($\Gamma/\omega_0 = 0.005$) to the red curve ($\Gamma/\omega_0 = 0.1$), the rate $K_{\rm loss}$, which determines the speed at which the system is attracted to its two semiclassical minima [6], is divided by two. Looking at Fig. 8(c), one could believe that the Wigner function negativity relaxes faster in the black case, but this is an impression which is due to the fact that the minimum of $\mathbf{M}(t)$ is reached earlier. For a more rigorous comparison of relaxation in the different cases, we have plotted, in Fig. 8(d), $\mathbf{M}(t)$ for different values of Γ when the cavity is initialized in all cases in the state corresponding to Fig. 8(a), upper graph, marked with a pink star, at time $t = 1740/\omega_0$. One can see that the relaxation of $\mathbf{M}(t)$ is similar in all cases, because this relaxation is set by the value of $\gamma^0_{\rm loss}$ (see Ref. [6]), which varies only weakly from one case to the other (for instance, one has $\gamma^0_{\rm loss} = 1.10\,10^{-4}\omega_0$ and $\gamma^0_{\rm loss} = 1.1610^{-4}\omega_0$ in the black and red cases, respectively). The facts mentioned above that ρ_p and $K_{\rm loss}$ vary a lot from the black to the red case whereas $\gamma^0_{\rm loss}$ is approximately unchanged deserves an explanation. The parameters ρ_p and $K_{\rm loss}$ describe two-photon resonance effects and the system is tuned at the two-photon resonant point $\omega_{\rm DQD} = 2\omega_0$ where ρ_p and $K_{\rm loss}$ present strong resonances. They are thus very sensitive to the value of Γ at this working point. This is not the case for the parameter $\gamma^0_{\rm loss}$ because it describes a single-photon effect which presents a resonance only at $\omega_{\rm DQD} = \omega_0$.

Figure 7 shows with magenta dots the minimum negativity $\min_t[\mathbf{M}(t)]$ of $W(t)$ over α, α^* and the time t, as a function of Γ. This quantity decreases more quickly with Γ than the amplitude of the semiclassical solution α^+_{av}. However, it is striking that a genuinely dissipative circuit such as a double quantum dot circuit is able to induce nonclassical cavity states thanks to the two-photon irreversible tunneling processes represented by $K_{\rm loss}$. Note that in Ref. [6], a two-photon dissipation term similar to ρ_p and a two-photon drive term similar to $K_{\rm loss}$ were obtained artificially by using an auxiliary cavity and two microwave tones. Photonic Schrödinger cats were obtained experimentally due to these effects. In our case, a single drive at $2\omega_0$ and the inclusion of a double dot in a single cavity are used to obtain these effects. For a typical cavity frequency $\omega_0 \approx 2\pi \times 5$ GHz, the required tunnel rates $\Gamma \approx 0.01\omega_0$ correspond to $0.2\,\mu$eV, a value which can be reached in practice [24,83]. With the simple protocol considered in this section, the photonic quantum superposition survives for a duration of the order of $8000/\omega_0 \simeq 0.25\ \mu$s which is much longer than the timescale $1/\Gamma = 100/\omega_0 \simeq$ 3 ns associated to dissipative tunneling between the dots and the normal reservoirs.

V. DISCUSSION

In this section, we discuss our results in the light of various recent references. Interestingly, Ref. [82] has proposed a method to combine the Lindblad description of a cavity coupled to a DQD and the Keldysh description of the dissipation provided by a bath of phonons coupled to the DQD. The aim of Ref. [82] is to study photon emission in the off-resonant regime $\omega_{\rm DQD} \neq \omega_0$ with the cavity driven at a frequency $\omega_d \sim \omega_0$ and the DQD dc voltage biased. Two-photon processes in K, $K_{\rm loss}$, $K_{\rm gain}$, and D are disregarded. Although this situation is physically different from the one we consider in Sec. IV, it is interesting to draw a technical comparison with our approach. In Ref. [82], the Keldysh framework is used to perform a diagrammatic calculation of the phonon-induced rates in the effective Lindblad equation of the cavity and DQD. This calculation is perturbative with respect to both the cavity-DQD coupling and the DQD-phonon bath coupling. Besides, the intrinsic cavity damping and the damping due to the fermionic leads of the DQD are implicitly assumed to be very small, so that they do not enter in the Keldysh diagrammatics and are added in the final Lindblad equation, as independent terms. Consequently, some of the phonon-induced rates have a denominator in $(\omega_{\rm DQD} \pm \omega_0)^2$, or $(\omega^2_{\rm DQD} - \omega^2_0)^2$, and thus diverge at $\omega_{\rm DQD} = \omega_0$ (see Eq. (22) and Fig. 4 of Ref. [82]). A regularization of these divergences by the system baths is missing and would require higher order perturbation series. In contrast, our approach is perturbative only in the cavity–double dot coupling. We do not have divergences in our effective rates at $\omega_{\rm DQD} = \omega_0$ or $\omega_{\rm DQD} = 2\omega_0$ because these are naturally regularized by the tunneling rate Γ to the fermionic leads, which appears in the mesoscopic Green's functions (72)–(74). This is essential to depict situations such as the one considered in Sec. IV.

In Sec. IV E 3, we have considered a system working point $\Delta\omega_{LR} = R(2\omega_0)$ such that the effective Kerr nonlinearity of the cavity K vanishes, and the effective two-photon dissipation $K_{\rm loss}$ and two-photon drive in ρ_p generate Schrödinger cats in a transient regime. Similarly, it has been shown experimentally with Josephson circuits that the combination of $K_{\rm loss}$ and ρ_p enables the autonomous preparation of Schrödinger cat states [6,7], but also the protection of these cats again certain types of decoherence [50]. This represents an important research direction in the context of the development of quantum computing schemes which require to fight calculation errors caused by decoherence. A cavity coupled to a double quantum dot could represent an alternative way to implement this "$K_{\rm loss}\&\rho_p$" qubit scheme. Interestingly, the preparation and protection of Schrödinger cat states can also be obtained in Josephson circuits by combing a Kerr nonlinearity K with ρ_p [47–49]. In our device, the required K can be obtained simultaneously with the two-photon loss $K_{\rm loss}$ ($K \neq 0$ and $K_{\rm loss} \neq 0$) or almost separately ($K \neq 0$, $K_{\rm loss} \to 0$) by working slightly away from the $\Delta\omega_{LR} = R(2\omega_0)$ resonance [see Figs. 4(b) and 4(d) and Eqs. (64) and (65)]. Therefore, it would also be interesting to investigate the potentialities of the cavity + double dot device to implement the "$K\&\rho_p$" qubit scheme or even a hybrid "$K_{\rm loss}\&K\&\rho_p$" qubit scheme.

Note that our formalism is suitable for describing experiments which involve quantum conductors with internal

degrees of freedom coupled to the cavity electric field. For the particular case of quantum conductors with no internal degrees of freedom, such as tunnel junctions or quantum point contacts, see, for instance, Refs. [44,46] for second-order effects in the light/matter coupling, and Ref. [45] for higher orders. In these references, the coupling of the source or drain of the conductors to the cavity electric field is favored by a galvanic coupling scheme (i.e., the source or drain of the device is directly connected to the cavity central conductor). We do not consider such a coupling but rather an electrostatic coupling of the mesoscopic circuit internal degrees of freedom to the cavity electric field because this is favored by most designs used in mesoscopic QED experiments where ac gates are placed between the circuit internal sites and the cavity central conductor. Our approach nevertheless takes into account photo-assisted dot-lead tunneling. For instance, in Ref. [23], the coefficient χ_2 reveals signatures of photo-assisted tunneling between a quantum dot and a superconducting contact.

VI. CONCLUSION

In this work, we have developed a quantum nonlinear description of mesoscopic QED experiments. More precisely, we have used a quantum path-integral approach to express the effective action of a microwave cavity with bare frequency ω_0, coupled to a generic mesoscopic circuit, and excited by a microwave drive at frequency $2\omega_0$. We have developed this action to fourth order in the cavity/circuit coupling. This development reveals photon/photon interactions mediated by the mesoscopic circuit. We have investigated the possibility to establish a Lindblad description of the cavity dynamics from the cavity action. This is always possible to third order in the light matter coupling. In this limit, the cavity is subject to a coherent photon pair drive [41] and a squeezing dissipation [42,43] mediated by the mesoscopic circuit. To fourth order in the light/matter coupling, we identify sufficient conditions in which a Markovian Lindblad description of the cavity dynamics is still possible. This condition has to be tested for a given circuit configuration by evaluating numerically different mesoscopic correlators. In the Lindblad framework, the mesoscopic circuit enables Kerr photon/photon interactions and two-photon loss/gain stochastic processes.

We have shown an example of application of our formalism to the case of a resonator coupled to a double quantum dot with normal metal contacts. The Lindblad condition is satisfied when the cavity and double dot are off-resonant (for single-photon exchange) and the dot-lead and dot-dot couplings weak enough ($\Gamma, t \ll \omega_0 - \omega_{\mathrm{DQD}}$). We have studied how nonlinear effects such as cavity squeezing and photonic Schrödinger cat states can occur, with a nontrivial influence of dissipative mesoscopic transport. In particular, quantum superpositions of photonic states can occur thanks to two-photon dissipation caused by tunneling processes inside the double dot circuit. The cavity squeezing effect also depends nontrivially on the dissipative tunnel rates between the dots and normal reservoirs (see Appendix F).

We anticipate that the quantum regime of mesoscopic QED conceals many more surprises which our approach can reveal. Indeed, our method can be extended straightforwardly to more complex circuit geometries with multiple quantum dots and ferromagnetic or superconducting reservoirs. The effect of Coulomb interactions inside the quantum dots also represents a rich field of investigation [66]. For simplicity, we have studied Lindbladian situations, which are Markovian by definition. However, our cavity action fully includes non-Markovian effects and it could be exploited in the non-Markovian regime by using a more general technical framework [40]. Therefore, our work should be instrumental to develop mesoscopic QED in the quantum nonlinear regime. Interestingly, the description of the effective dynamics of microwave cavities coupled to dissipative Josephson circuits is also an important topic which lacks of systematic approaches beyond the second order in the light/matter interaction [84,85]. Our path-integral approach could be used to tackle this problem.

ACKNOWLEDGMENTS

Z.L. acknowledges support from Agence Nationale de la Recherche Project ENDURANCE and EMERGENCES Grant ENDURANCE of Ville de Paris. T.K. acknowledges support from Quantera Project SuperTop.

APPENDIX A: DETAILS ON THE DERIVATION OF THE CAVITY EFFECTIVE ACTION

Here, we give more details on the derivation of Eqs. (28)–(45). The drive at frequency $2\omega_0$ is not resonant with the cavity and will affect the photonic dynamics only indirectly thanks to the nonlinearity of the mesoscopic circuit. To emphasize this fact and simplify the calculation of the cavity effective action, it is convenient to make a displacement of the cavity fields

$$\begin{bmatrix}\phi_{cl}(t)\\ \phi_q(t)\end{bmatrix} = \begin{bmatrix}\varphi_{cl}(t)\\ \varphi_q(t)\end{bmatrix} + \begin{bmatrix}\int_\omega \sqrt{2}\varepsilon^*_{ac}(\omega)\mathcal{G}^A_0(\omega)e^{i\omega t}\\ 0\end{bmatrix} \tag{A1}$$

with the cavity drive ε_{ac} defined temporally in Eq. (3) and $\mathcal{G}^A_0$ being the bare cavity Green's function defined in Eq. (37). In this framework, the action of the system becomes

$$Z = \int d[\bar\phi, \phi] e^{iS^0_{\mathrm{cav}}(\bar\phi,\phi)} \int d[\bar\psi, \psi] e^{iS_{\mathrm{meso}}(\bar\varphi,\varphi,\bar\psi,\psi)} \tag{A2}$$

with S^0_{cav} defined in Eq. (19),

$$S_{\mathrm{meso}}(\bar\phi, \phi, \bar\psi, \psi) = \int_{t,t'} \bar\psi(t)[\check G^{-1}(t,t') - \check v^{\bar\phi,\phi}_\Sigma(t,t')]\psi(t'), \tag{A3}$$

$$\check v^{\bar\phi,\phi}_\Sigma(t,t') = [\check v(\bar\phi,\phi,t) + \check v_{ac,1}(t) + \check v^\dagger_{ac,1}(t)]\delta(t-t'), \tag{A4}$$

and

$$\check v_{ac,1}(t) = \frac{\check g}{2}\left[\varepsilon_p \mathcal{G}^R_0(2\omega_0)e^{-i2\omega_0 t} + \varepsilon^*_p \mathcal{G}^R_0(-2\omega_0)e^{i2\omega_0 t}\right]. \tag{A5}$$

In Eqs. (A3)–(A5), the ac drive now modifies directly the potential seen by the electrons of the mesoscopic circuit. The coefficients in $\mathcal{G}^R_0$ in Eq. (A5) express how the ac drive is seen by electrons after a transduction by the cavity. They lead to the occurrence of the factor t_0 in Eq. (35).

To eliminate the electronic degrees of freedom from Eq. (A2), we perform a Gaussian integration of (A2) with respect to the $\bar\psi$ and ψ fields. This Gaussian integration is

possible because, in the absence of Coulomb interactions, the system action is quadratic with respect to the electronic fields. This gives

$$Z = \int d[\bar{\phi}, \phi] e^{iS^0_{\rm cav}(\bar{\phi},\phi)} \Xi(\bar{\phi}, \phi) \tag{A6}$$

with

$$\Xi(\bar{\phi}, \phi) = \det_{t,k,d}[\check{1} - \check{m}] \tag{A7}$$

and

$$\check{m} = \check{G} \circ \check{v}^{\bar{\phi},\phi}_{\Sigma}. \tag{A8}$$

Above, $\circ$ denotes a convolution on the time variables and a matrix product on the mesoscopic orbital degrees of freedom, and $\det_{t,k,d}$ is a generalized determinant on the time, Keldysh, and orbital spaces which is defined such that [86]

$$\ln[\Xi(\bar{\phi}, \phi)] = -\int_t \mathrm{Tr}_{k,d}\left[\check{m}(t,t) + \frac{\check{m} \circ \check{m}|_{t,t}}{2} + \frac{\check{m} \circ \check{m} \circ \check{m}|_{t,t}}{3} + \cdots\right]. \tag{A9}$$

In this work, we build a perturbation theory where the development parameter is the matricial function $\check{m}$ which appears in Eq. (A9).

The next step is to express Eq. (A9) in terms of dot Green's functions. This can generate many terms with a complex structure, but significant simplifications can be performed in the limit where the dressed cavity has a sufficient finesse. For brevity, we only discuss the development of the first- and second-order terms

$$C_1 = -\int_t \mathrm{Tr}_{k,d} \check{m}(t,t)_{\varepsilon_p=0} \tag{A10}$$

and

$$C_2 = -\int_t \mathrm{Tr}_{k,d}[\check{m} \circ \check{m}|_{t,t}/2]_{\varepsilon_p=0} \tag{A11}$$

in Eq. (A9), in the absence of the $2\omega_0$ drive ($\varepsilon_p = 0$).

Let us first calculate C_1. From the definitions of $\check{m}$ and $\check{v}^{\bar{\phi},\phi}_{\Sigma}$, one has

$$C_1 = -\int_{t,t'} \mathrm{Tr}_{k,d}[\check{G}(t,t')\check{v}(\bar{\phi}, \phi, t')]. \tag{A12}$$

Then, using the definition (27) of $\check{v}$ in terms of fermionic fields and the expression (23) of $\check{G}$ in terms of Keldysh components, we obtain

$$\begin{aligned} -\sqrt{2}C_1 = &\sum_d g_d\big(\tilde{G}^{d,d}_r(t=0) + \tilde{G}^{d,d}_a(t=0)\big) \\ &\times \int_t (\bar{\varphi}_{cl}(t) + \varphi_{cl}(t)) \\ &+ \sum_d g_d \tilde{G}^{d,d}_K(t=0) \int_t (\bar{\varphi}_q(t) + \varphi_q(t)). \end{aligned}$$

Using the general relation [87] $\tilde{G}^{d,d}_r(t=0) + \tilde{G}^{d,d}_a(t=0) = 0$ and the definition (26) of $\tilde{G}^{d,d}_K$, one can check

$$C_1 = -\frac{i}{\sqrt{2}} \sum_d g_d (2n_{d,0} - 1) \int_t (\bar{\varphi}_q(t) + \varphi_q(t)), \tag{A13}$$

where $n_{d,0} = \langle \hat{c}^\dagger_d \hat{c}_d \rangle_{\check{g}=0}$ is the average occupation of level d in the absence of light/matter coupling. A comparison of this term with Eq. (20) shows that C_1 corresponds to a cavity dc drive

$$H^{\rm eff}_{cav,1} = \sum_d g_d \left(n_{d,0} - \frac{1}{2}\right)(\hat{a}^\dagger + \hat{a}), \tag{A14}$$

which can be disregarded in our study due to its nonresonant nature.

We now calculate C_2. From the definitions of $\check{m}$ and $\check{v}^{\bar{\phi},\phi}_{\Sigma}$, one has

$$C_2 = -\int_{t,t'} \mathrm{Tr}_{k,d}[\check{G}(t,t')\check{v}(\bar{\phi}, \phi, t')\check{G}(t',t)\check{v}(\bar{\phi}, \phi, t)]/4. \tag{A15}$$

Using the definition (27) of $\check{v}$ in terms of fermionic fields and introducing Fourier transforms, one gets

$$\begin{aligned} C_2 = &-\iint_{\omega_1,\omega_2} \mathrm{Tr}_{k,d}[\check{G}(\omega_1)\check{g}\bar{\phi}_\Sigma(\omega_3 - \omega_1)\check{G}(\omega_3) \\ &\qquad \times \check{g}\bar{\phi}_\Sigma(\omega_1 - \omega_3)]/4 \\ &- \iint_{\omega_1,\omega_2} \mathrm{Tr}_{k,d}[\check{G}(\omega_1)\check{g}\bar{\phi}_\Sigma(\omega_3 - \omega_1)\check{G}(\omega_3)\check{g}\phi_\Sigma(\omega_3 - \omega_1)]/4 \\ &- \iint_{\omega_1,\omega_2} \mathrm{Tr}_{k,d}[\check{G}(\omega_1)\check{g}\phi_\Sigma(\omega_1 - \omega_3)\check{G}(\omega_3)\check{g}\bar{\phi}_\Sigma(\omega_1 - \omega_3)]/4 \\ &- \iint_{\omega_1,\omega_2} \mathrm{Tr}_{k,d}[\check{G}(\omega_1)\check{g}\phi_\Sigma(\omega_1 - \omega_3)\check{G}(\omega_3)\check{g}\phi_\Sigma(\omega_3 - \omega_1)]/4 \end{aligned} \tag{A16}$$

with

$$\phi_\Sigma(\omega_3 - \omega_1) = \phi_{cl}(\omega_3 - \omega_1)\check{\sigma}_0 + \phi_q(\omega_3 - \omega_1)\check{\sigma}_1 \tag{A17}$$

and

$$\bar{\phi}_\Sigma(\omega_3 - \omega_1) = \bar{\phi}_{cl}(\omega_3 - \omega_1)\check{\sigma}_0 + \bar{\phi}_q(\omega_3 - \omega_1)\check{\sigma}_1. \tag{A18}$$

Assuming that the dressed cavity has a good quality factor ($\Lambda_0^{\rm app} = \Lambda_0 + \Delta\Lambda_0 \ll \omega_0$ has to be checked *a posteriori*), the terms $\phi_\Sigma(\omega_1 - \omega_3)$ and $\phi_\Sigma(\omega_3 - \omega_1)$ have a weak overlap and therefore the first and fourth lines of the above expression, which contains products $\bar{\phi}_{cl(q)}\bar{\phi}_{cl[q]}$ or $\phi_{cl(q)}\phi_{cl(q)}$, are negligible. A change of frequency variables in the remaining terms (which contain contributions in $\bar{\phi}_{cl(q)}\phi_{cl[q]}$ only) gives

$$\begin{aligned} C_2 = &-\iint_{\omega_1,\omega} \mathrm{Tr}_{k,d}[\check{G}(\omega_1)\check{g}\bar{\phi}_\Sigma(\omega)\check{G}(\omega + \omega_1)\check{g}\phi_\Sigma(\omega)]/4 \\ &- \iint_{\omega_1,\omega} \mathrm{Tr}_{k,d}[\check{G}(\omega_1)\check{g}\phi_\Sigma(\omega)\check{G}(\omega_1 - \omega)\check{g}\bar{\phi}_\Sigma(\omega)]/4. \end{aligned} \tag{A19}$$

Then, we assume that the dressed cavity linewidth is much smaller than the mesoscopic resonances linewidth ($\Lambda_0 + \Delta\Lambda_0 \ll \Gamma$ has to be checked *a posteriori*, with Γ the order of magnitude of the tunnel rates to the mesoscopic reservoirs). In this case, the terms in $\check{G}$ in the above integral vary very

slowly in the frequency area $\omega_0 - \Lambda_0^{\rm app} \lesssim \omega \lesssim \omega_0 + \Lambda_0^{\rm app}$, where $\phi_\Sigma(\omega)$ and $\bar\phi_\Sigma(\omega)$ contribute significantly to the cavity action, and one can thus use $\omega \simeq \omega_0$ in these terms. This gives

$$C_2 = -\iint_{\omega_1,\omega} \mathrm{Tr}_{k,d}[\check G(\omega)\check g\bar\phi_\Sigma(\omega_1)\check G(\omega_0+\omega)\check g\phi_\Sigma(\omega_1)]/4 - \iint_{\omega_1,\omega} \mathrm{Tr}_{k,d}[\check G(\omega)\check g\phi_\Sigma(\omega_1)\check G(\omega-\omega_0)\check g\bar\phi_\Sigma(\omega_1)]/4. \tag{A20}$$

Finally, we can come back to the time representation for the cavity fields

$$C_2 = -\iint_{\omega,t} \mathrm{Tr}_{k,d}[\check G(\omega)\check g\bar\phi_\Sigma(t)\check G(\omega_0+\omega)\check g\phi_\Sigma(t)]/4 - \iint_{\omega,\omega} \mathrm{Tr}_{k,d}[\check G(\omega)\check g\phi_\Sigma(t)\check G(\omega-\omega_0)\check g\bar\phi_\Sigma(t)]/4. \tag{A21}$$

A rearrangement of these terms leads to an action contribution similar to that of Eq. (29), with fields $\bar\varphi$, φ replaced by $\bar\phi$, ϕ. A similar treatment can be performed for higher order terms of Eq. (A9) and terms which depend on ε_p. For instance, the contribution in g^4 corresponds to six terms similar to those of Eq. (A21). We finally obtain, after some algebra and term regrouping, a cavity effective Schwinger-Keldysh partition function $Z = \int d[\bar\phi,\phi]e^{iS^{\rm eff}_{\rm cav}(\bar\phi,\phi)}$ with $S^{\rm eff}_{\rm cav}$ defined in Eq. (28). The final step is to come back to an expression of the cavity action with the fields $\bar\varphi$, φ. We disregard terms of order $g^4\varepsilon_p$, since we assume that both g^4 and ε_p are small. In this case, one obtains $Z = \int d[\bar\varphi,\varphi]e^{i(S^{\rm eff}_{\rm cav}(\bar\varphi,\varphi)+\Delta\tilde S_{ac}(\bar\varphi,\varphi))}$, where $\Delta\tilde S_{ac}(\bar\varphi,\varphi)$ is a drive term similar to the term $\Delta S_{ac}(\bar\varphi,\varphi)$ of Eq. (20), but with an amplitude ε_p which has a renormalization in $g^2\varepsilon_p$. However, since this ac drive is nonresonant with the cavity, one can disregard $\Delta\tilde S_{ac}$. Therefore, one can use $Z \simeq \int d[\bar\varphi,\varphi]\exp[iS^{\rm eff}_{\rm cav}(\bar\varphi,\varphi)]$. In particular, one gets the expression

$$\mathcal{A} = i\begin{bmatrix} \mathcal{N}_{cl,cl,cl,cl} & \mathcal{N}_{cl,cl,cl,q} & \mathcal{N}_{cl,cl,q,q} \\ \mathcal{N}_{cl,q,cl,cl} & \mathcal{N}_{cl,q,cl,q} & \mathcal{N}_{cl,q,q,q} \\ \mathcal{N}_{q,q,cl,cl} & \mathcal{N}_{q,q,cl,q} & \mathcal{N}_{q,q,q,q} \end{bmatrix} \tag{A22}$$

for the matrix which occurs in the expression (38), with coefficients $\mathcal{N}_{f,f',l,l'}$ defined in Eq. (45). Using the cyclic property of the trace in Eq. (45) and the properties $\tilde G_K(\omega) = -\tilde G_K(\omega)^\dagger$ and $\tilde G_a(\omega) = \tilde G_r(\omega)^\dagger$, one can check that there exists relations between the different components of $\mathcal{A}$ in Eq. (A22) so that one finally gets expression (39).

APPENDIX B: SEMICLASSICAL DESCRIPTION OF MESOSCOPIC QED

1. Direct semiclassical description of mesoscopic QED

It is useful to reconsider the problem of mesoscopic QED with a direct semiclassical approach (without the path-integral formulation) in order to gain more physical insight into the new coefficients χ_4 and U_{cl} which appear in Eqs. (32) and (38). Equation (1) gives the photonic equation of motion in the Heisenberg picture:

$$\frac{d}{dt}\hat a(t) = -i\omega_0\hat a(t) - \frac{i}{\hbar}\sum_d g_d\hat n_d(t) - \frac{\Lambda_0}{2}\hat a(t) - i\varepsilon_{ac}(t). \tag{B1}$$

In a semiclassical picture, the operator $\hat a(t)$ in the above equation can be treated as a classical quantity $a(t) = \hat a(t) = \langle\hat a(t)\rangle$. In this case, the average electron number operator $\langle\hat n_d(t)\rangle = \langle\hat c_d^\dagger(t)\hat c_d(t)\rangle$ in orbital d can be calculated as the response to the "classical" excitations $g_{d'}(a^\dagger(t)+a(t))$, with $d' \in [1,N]$, which we will write in a matrix form as

$$\tilde E_{ac}(t) = \tilde g(a^\dagger(t)+a(t)). \tag{B2}$$

At this stage, although $a(t)$ is expected to have a dominant contribution in $e^{-i\omega_0 t}$, it is essential to take into account weak components in $e^{\pm i2\omega_0 t}$ to describe the effect of the drive in β_p on $\langle\hat n_d(t)\rangle$. It is sufficient to estimate these components from Eq. (B1) treated to order 0 in g, because this is enough to obtain a $\beta_p g^3$ contribution to the photonic field, as we will see below. Hence, we use

$$\tilde E_{ac}(t) = \tilde g(\alpha e^{-i\omega_0 t} + \alpha^* e^{i\omega_0 t} + \mathrm{Re}[t_0\varepsilon_p e^{-i2\omega_0 t}/2]) \tag{B3}$$

with t_0 defined by Eq. (36). The amplitude α is not specified since it must be determined self-consistently from Eq. (B1) and the response of the average dot charges to $\tilde E_{ac}(t)$. From the Keldysh description of mesoscopic transport [77], this response is given by

$$\sum_d g_d\langle\hat n_d(t)\rangle = -i\mathrm{Tr}_d[\tilde g\tilde{\mathbf G}_<(t,t)], \tag{B4}$$

where the lesser Green's function of the dots $\tilde{\mathbf G}_<$ in the presence of $\tilde E_{ac}(t)$ can be expressed as

$$\tilde{\mathbf G}_<(t,t) = \iiint \frac{d\omega}{2\pi}dt_1dt_2e^{-i\omega(t_1-t_2)} \times \tilde{\mathbf G}_r(t,t_1)\tilde\Sigma^<(\omega)\tilde{\mathbf G}_a(t_2,t). \tag{B5}$$

Above, $\tilde\Sigma^<(\omega)$ is the lesser self-energy of the dots illustrated in Sec. IV B for the double dot case. The mesoscopic retarded and advanced Green's functions $\tilde{\mathbf G}_{r(a)}$ in the presence of $\tilde E_{ac}(t)$ can be calculated in terms of the unperturbed mesoscopic Green's functions $\tilde G_{r(a)}$ defined in Sec. III A by using the Dyson equation

$$\tilde{\mathbf G}_J(t,t') = \tilde G_J(t,t') + \int\frac{dt_1}{\hbar}\tilde G_J(t,t_1)\tilde E_{ac}(t_1)\tilde{\mathbf G}_J(t_1,t') \tag{B6}$$

with $J \in r(a)$.

The combination of Eqs. (B4)–(B6) gives, by keeping only resonant contributions in $e^{-i\omega_0 t}$,

$$\sum_d g_d\langle\hat n_d\rangle \simeq (\alpha\chi_2 + 2\alpha|\alpha|^2\chi_4 + i\alpha^* U_{cl})e^{-i\omega_0 t}. \tag{B7}$$

Tedious algebra is necessary to identify the coefficients which appear in Eq. (B7) with the correlation functions U_{cl} and χ_4 defined in the main text, especially in the multiorbital case $N > 1$. Equation (B7) shows that χ_2 is the linear response function of the dots charge to the excitation in $\alpha e^{-i\omega_0 t}$, and χ_4 is the second-order response function to the same excitation,

whereas U_{cl} appears as a transduction coefficient for the field component in $\alpha^* e^{i\omega_0 t}$ into a resonant term in $e^{-i\omega_0 t}$ thanks to the energy provided by the drive in ε_p. One can finally inject Eq. (B7) into the statistical average of Eq. (B1) to obtain

$$0 = \alpha^* U_{cl} - \left(i\chi_2 + \frac{\Lambda_0}{2} + 2i|\alpha|^2\chi_4\right)\alpha. \tag{B8}$$

For this last step, we have used the resonant approximation $a(t) \simeq \alpha e^{-i\omega_0 t}$ in Eq. (B1) and disregarded the term in $\varepsilon_{ac}(t)$ in the right member of (B1) because it is not resonant with the cavity. One can see along this calculation that ε_p plays a crucial role in intermediary steps of the calculation for the description of two-photon processes, but its direct contribution to (B8) can be disregarded. A similar fact happens with the path-integral approach, where ε_p produces indirectly the $S_g^{(3)}(t)$ term, whereas its direct contribution $\Delta S_{ac}(t)$ can be disregarded from the effective action $S_{\rm cav}^{\rm eff}(t)$ in the resonant approximation. Note that Eq. (B8) is in full agreement with the result given by a direct calculation of the semiclassical cavity steady states with the path-integral description (see Appendix B 2).

2. Semiclassical photonic amplitudes given by the path-integral description

The possible semiclassical photonic amplitudes of the cavity in stationary conditions can also be obtained by looking for the saddle points of the cavity effective action [40]. Since the action (28) vanishes for $\varphi_{cl} = 0$, $\bar\varphi_{cl} = 0$, a semiclassical solution for the cavity field can be found at $\varphi_q = 0$, $\bar\varphi_q = 0$ and values of φ_{cl} and $\bar\varphi_{cl}$ such that $\partial(S)/\partial\bar\varphi_q(t)|_{\varphi_q=0,\bar\varphi_q=0} = 0$. This gives

$$-\sqrt{2}\varepsilon_{ac}(t) = \left(i\partial_t - \omega_0 + \frac{i\Lambda_0}{2}\right)\varphi_{cl} - \chi_2\varphi_{cl} - ie^{-2i\omega_0 t}U_{cl}\bar\varphi_{cl} - \chi_4\bar\varphi_{cl}\varphi_{cl}\varphi_{cl}. \tag{B9}$$

One can disregarded $\varepsilon_{ac}(t)$ from the left member of Eq. (B9) because it is not directly resonant with the cavity. Hence, one can expect a semiclassical solution $\varphi_{sc} = \sqrt{2}\alpha_{sc}e^{i(\varphi_{sc}-\omega_0 t)}$ such that

$$\left(U_{cl}e^{-2i\varphi_{sc}} - \frac{\Lambda_0}{2} - i\chi_2 - 2i\chi_4|\alpha_{sc}|^2\right)\alpha_{sc} = 0 \tag{B10}$$

with α_{sc} the semiclassical value of $\hat a$. Equation (B10) is in full agreement with the semiclassical Eq. (B8) if $\alpha = \alpha_{sc}$ is used. This equation is also similar to Eq. (83) on the average photons amplitude α_{av} obtained from the Lindblad description of the cavity dynamics, up to the term in $\Delta\Lambda_{0,4}$ which is not present in Eq. (B10). This discrepancy is due to the fact that the equation on α_{sc} is obtained by disregarding quantum fluctuations of the cavity occupation.

APPENDIX C: ACTION ASSOCIATED TO A LINDBLAD EQUATION

Following Ref. [88], the action corresponding to a Lindblad equation with the form (46) can be expressed as

$$S = \int_t (\bar\varphi_+(t)i\partial t\varphi_+(t) - \bar\varphi_-(t)i\partial t\varphi_-(t) - i\mathcal{L}(t)) \tag{C1}$$

with $\varphi_\pm = \frac{1}{\sqrt{2}}(\varphi_{cl} \pm \varphi_q)$, $\bar\varphi_\pm = \frac{1}{\sqrt{2}}(\bar\varphi_{cl} \pm \bar\varphi_q)$, and

$$\begin{aligned} -i\mathcal{L}(t) = &- H_{\rm cav}^{\rm eff}[\bar\varphi_+(t), \varphi_+(t)] + H_{\rm cav}^{\rm eff}[\bar\varphi_-(t), \varphi_-(t)] \\ &- i\sum_j \gamma_j \hat L_j[\bar\varphi_+, \varphi_+]\hat L_j^\dagger[\bar\varphi_-, \varphi_-] \\ &+ \frac{i}{2}\sum_{j,s\in\{+,-\}} \gamma_j \hat L_j^\dagger[\bar\varphi_s, \varphi_s]\hat L_j[\bar\varphi_s, \varphi_s]. \end{aligned} \tag{C2}$$

This leads to Eqs. (49), (61), and (62) of the main text. Note that this result is valid even when the dissipative rates γ_j and the Hamiltonian $H_{\rm cav}^{\rm eff}$ are time dependent.

APPENDIX D: LINK BETWEEN THE DIRECT DENSITY MATRIX APPROACH AND THE PATH-INTEGRAL APPROACH TO SECOND ORDER IN g

To show that the Lindblad Eqs. (12) and (67) obtained with the direct density matrix approach and the path-integral approach, respectively, agree to second order in g, one must establish the relation between the parameters χ_A, χ_B and χ_2, λ_2 which occur in these equations. Note that χ_2 and λ_2 have a frequency dependence which is omitted in the main text where we use $\chi_2 = \chi_2(\omega_0)$ and $\lambda_2 = \lambda_2(\omega_0)$. For our present purpose, it is convenient to use the inverse Fourier transform of these quantities, defined generally as $f(t) = \int_{-\infty}^{+\infty}\frac{d\omega_0}{2\pi}f(\omega_0)e^{-i\omega_0 t}$. One can use the general relation

$$\int_{-\infty}^{+\infty}\frac{d\omega}{2\pi}a(\omega+\omega_0)b(\omega) = \int_{-\infty}^{+\infty} dt\, a(t)b(-t)e^{i\omega_0 t}, \tag{D1}$$

where a and b are two generic functions, to re-express Eqs. (30) and (31) as

$$\chi_2(t) = -\frac{i}{2}\mathrm{Tr}_d[\tilde G_K(t)\tilde g\tilde G_a(-t)\tilde g + \tilde G_K(-t)\tilde g\tilde G_r(t)\tilde g], \tag{D2}$$

$$\begin{aligned} \lambda_2(t) = &-\frac{i}{2}\mathrm{Tr}_d[\tilde G_K(-t)\tilde g\tilde G_K(t)\tilde g \\ &+ \tilde G_a(-t)\tilde g\tilde G_r(t)\tilde g + \tilde G_r(-t)\tilde g\tilde G_a(t)\tilde g]. \end{aligned} \tag{D3}$$

At this stage, it is convenient to define the lesser and greater fermionic Green's functions

$$G_<^{d,d'}(t) = i\langle\hat c_{d'}^\dagger(0)\hat c_d(t)\rangle \tag{D4}$$

and

$$G_>^{d,d'}(t) = -i\langle\hat c_d(t)\hat c_{d'}^\dagger(0)\rangle \tag{D5}$$

to re-express definitions (24)–(26) as

$$G_r^{d,d'}(t) = \theta(t)(G_>^{d,d'}(t) - G_<^{d,d'}(t)), \tag{D6}$$

$$G_a^{d,d'}(t) = \theta(-t)(G_<^{d,d'}(t) - G_>^{d,d'}(t)), \tag{D7}$$

and

$$G_K^{d,d'}(t) = G_<^{d,d'}(t) + G_>^{d,d'}(t). \tag{D8}$$

Then, using Eqs. (D6)–(D8), one can rewrite Eqs. (D2) and (D3) as

$$\chi_2(t) = i\theta(t)\mathrm{Tr}_d[\tilde G_<(t)\tilde g\tilde G_>(-t)\tilde g - \tilde G_>(t)\tilde g\tilde G_<(-t)\tilde g], \tag{D9}$$

$$\lambda_2(t) = -i\mathrm{Tr}_d[\tilde G_<(-t)\tilde g\tilde G_>(t)\tilde g + \tilde G_>(-t)\tilde g\tilde G_<(t)\tilde g]. \tag{D10}$$

Since we consider a noninteracting case, one can use the Wick theorem to re-express the above equations in terms of charge correlators [71]. Indeed, using the operator $\hat{N}(t)$ of Eq. (6), one finds

$$\langle \hat{N}(t)\hat{N}(0)\rangle = \langle \hat{N}\rangle^2 + \mathrm{Tr}_d[\tilde{G}_<(-t)\tilde{g}\tilde{G}_>(t)\tilde{g}], \tag{D11}$$

$$\langle \hat{N}(0)\hat{N}(t)\rangle = \langle \hat{N}\rangle^2 + \mathrm{Tr}_d[\tilde{G}_<(t)\tilde{g}\tilde{G}_>(-t)\tilde{g}]. \tag{D12}$$

This leads to

$$\chi_2(t) = i\theta(t)(\langle \hat{N}(0)\hat{N}(t)\rangle - \langle \hat{N}(t)\hat{N}(0)\rangle), \tag{D13}$$

$$\lambda_2(t) = -i(\langle \hat{N}(0)\hat{N}(t)\rangle + \langle \hat{N}(t)\hat{N}(0)\rangle - 2\langle \hat{N}\rangle^2). \tag{D14}$$

A comparison of these equations with the definitions (14) and (15) of $\chi_A(t)$ and $\chi_B(t)$ gives, in the frequency domain,

$$\chi_2(\omega_0) = \chi_B(\omega_0) - \chi_A(\omega_0), \tag{D15}$$

$$\lambda_2(\omega_0) = 2i(\mathrm{Im}[\chi_A(\omega_0) + \chi_B(\omega_0)] + \langle \hat{N}\rangle^2\delta(\omega_0)). \tag{D16}$$

This proves the relations (70) and (71) of the main text and the agreement between the Lindblad Eqs. (12) and (67) at second order in g.

APPENDIX E: ANALYTICAL CALCULATION OF THE WIGNER FUNCTION TO THIRD ORDER IN g

The definition (77) of the Wigner function involves the correlation function $\chi(t,\beta,\beta^*) = \langle e^{\beta a_l^\dagger - \beta^* a_l}\rangle_t$. From the expression of the effective Hamiltonian $H_{\mathrm{cav}}^{\mathrm{eff}}$ and the jump operators $\hat{L}_j$, one can check that χ follows [40]

$$\begin{aligned}\frac{\partial}{\partial t}\chi = &-i\Delta\omega_0(-\beta\partial_\beta + \beta^*\partial_{\beta^*})\chi - \gamma_+\frac{\beta\beta^*}{2}\chi \\ &- \frac{\gamma_-}{2}(\beta^*\partial_{\beta^*} + \beta\partial_\beta)\chi - 2\rho_p\beta^*\partial_\beta\chi - 2\rho_p^*\beta\partial_{\beta^*}\chi \\ &- \frac{\beta^2}{2}\gamma_p e^{-i\varphi_p}\chi - \frac{\beta^{*2}}{2}\gamma_p e^{i\varphi_p}\chi.\end{aligned} \tag{E1}$$

For compactness, we note $\frac{\partial}{\partial\beta} = \partial_\beta$ and $\frac{\partial}{\partial\beta^*} = \partial_{\beta^*}$. The above equation is a first-order differential equation which is more convenient to solve than the second-order differential equation (77). It is then straightforward to Fourier transform χ to obtain $W(t)$.

APPENDIX F: PARAMETRIC CONTROL OF THE SQUEEZING EFFECT

This Appendix discusses how the photonic squeezing effect of Sec. IV D depends on the double dot parameters. Figure 9 shows the cavity field quadratures $\Delta X_\pm$ versus the orbital detuning $\Delta\omega_{RL} = \omega_R - \omega_L$ [Fig. 9(a)], versus Γ [Fig. 9(b)], and versus the cavity drive amplitude β_p [Fig. 9(c)] for a case where the single- and two-photon resonances at $\Delta\omega_{RL} = R(\omega_0)$ and $\Delta\omega_{RL} = R(2\omega_0)$ are allowed. The results given by the full expressions (81) and (82) of A and B are shown with full lines. For reference, the variance

$$\Delta X_2 = \frac{1}{2}\sqrt{\frac{\Lambda_0(1+2n_B) - \mathrm{Im}[\lambda_2]}{\Lambda_0 - 2\,\mathrm{Im}[\chi_2]}} \tag{F1}$$

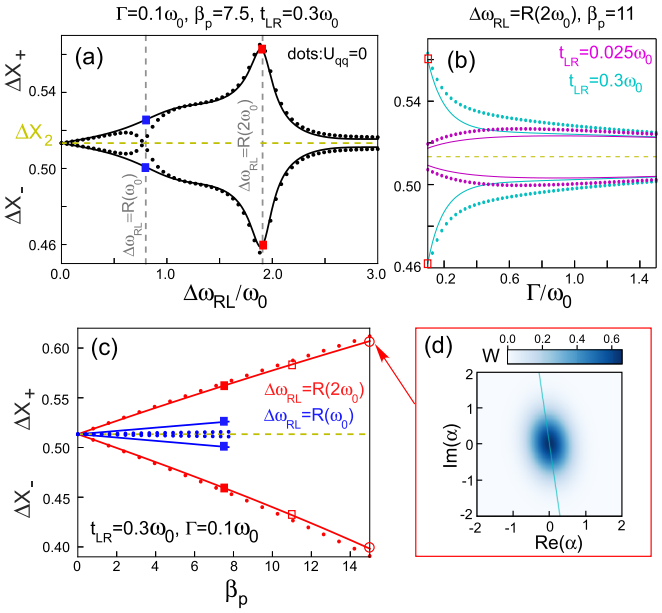

FIG. 9. [(a)–(c)] Cavity field quadratures $\Delta X_\pm$ vs $\Delta\omega_{RL}$, Γ, and β_p respectively. In panel (a), we use $t_{LR} = 0.3\omega_0$, $\Gamma = 0.1\omega_0$, and $\beta_p = 7.5$. In panel (b), we use $t_{LR} = 0.3\omega_0$ (cyan lines) or $t_{LR} = 0.025\omega_0$ (magenta lines), $\Delta\omega_{RL} = R(2\omega_0)$, and $\beta_p = 11$. In panel (c), we use $t_{LR} = 0.3$, $\Gamma = 0.1\omega_0$, and $\Delta\omega_{RL} = R(2\omega_0)$ (red lines) or $\Delta\omega_{RL} = R(\omega_0)$ (blue lines). The other parameters are the same as in Fig. 3 with $\omega_{av} = 0$ and $g_L = 0.01\omega_0$. The full lines correspond to the result given by the full expressions (81) and (82) of A and B, whereas the dotted lines omit the contribution of γ_p (or equivalently U_{qq}). For reference, the second-order variance ΔX_2 for an empty cavity (corresponding to the case for $g_L = 0$) is also shown as a dashed yellow line. The vertical dashed gray lines in panel (a) indicate the resonances $\Delta\omega_{RL} = R(\omega_0)$ and $\Delta\omega_{RL} = R(2\omega_0)$. The blue and red squares indicate working points which are common to panels (a), (b), and (c). In panel (c), the plots are restricted to the range where $\gamma_{\mathrm{loss}} > 0$ and $\gamma_{\mathrm{gain}} > 0$, which is narrower in the case $\Delta\omega_{RL} = R(\omega_0)$ (blue curves). (d) Squeezed cavity Wigner function for the working point corresponding to the empty red circles in panel (c). The major axis of the Wigner function is shown as a blue line.

of the cavity field to second order in g_L is also shown as a yellow line. One gets a squeezing effect ($\Delta X_- < \Delta X_2 < \Delta X_+$), which is maximal at $\Delta\omega_{RL} = R(2\omega_0)$ [Fig. 9(a)]. As visible in [Fig. 9(b)], for $t_{LR} = 0.3$ (cyan full line), squeezing decreases with Γ. One could expect that higher values of Γ are always detrimental to squeezing. However, for a small value of t_{LR} (magenta full lines), the squeezing effect finds a local maximum for a value of Γ which can be quite significant [$\Gamma \sim 0.9\omega_0$ in Fig. 9(b)].

To determine the role of the parameter U_q (or γ_p), we show with dotted lines in Figs. 9(a)–(c) the cavity field quadratures given by Eqs. (81) and (82) with γ_p omitted ($\gamma_p = 0$). For the moderate tunnel rate Γ used in Fig. 9(a), the full and dotted lines coincide around $\Delta\omega_{RL} = R(2\omega_0)$ but not near the single-photon resonance $\Delta\omega_{RL} = R(\omega_0)$. For $\Delta\omega_{RL} = R(\omega_0)$, the dissipative term in U_q is responsible for an increase of the squeezing effect, in spite of its dissipative nature [42,43]. Such an effect is allowed by Eq. (82). To see an effect of U_q on the squeezing at the working point $\Delta\omega_{RL} = R(2\omega_0)$,

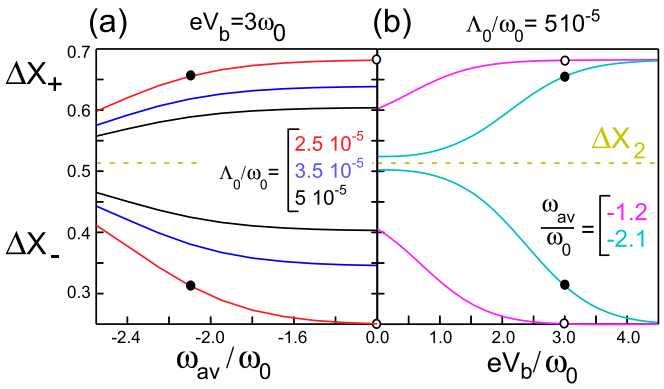

FIG. 10. Cavity field quadratures $\Delta X_\pm$ vs $\omega_{av} = (\omega_R + \omega_L)/2$ (a) and vs the bias voltage V_b (b) for $\Delta\omega_{RL} = 2\omega_0$, $t_{LR} = 0.1\omega_0$, $g_L = 0.01\omega_0$, and $\beta_p = 200$. The other parameters are the same as in Fig. 3. Panel (a) considers different cavity damping rates $\Lambda_0/(10^{-5}\omega_0) = 2.5$, 3.5, and 5 with red, blue, and black lines. Panel (b) shows results for average dot orbital energies $\omega_{av}/\omega_0 = -2.1$ (cyan lines) and $\omega_{av}/\omega_0 = -1.2$ (green lines). The circles indicate working points common to panels (a) and (b). For reference, the second-order variance $\Delta X_2 = \sqrt{1 + 2n_B}/2$ for a decoupled cavity ($g_L = 0$) is also shown as a dashed yellow line. It is independent of the value of Λ_0.

it is necessary to increase the value of Γ [see Fig. 9(b)]. In this case, U_q causes a decrease of the squeezing amplitude. To summarize, the dissipative term in U_q can either increase or decrease the squeezing effect, depending on the regime of parameters. Nevertheless, to maximize the squeezing effect, it is advantageous to use the regime $\Delta\omega_{RL} = R(2\omega_0)$ and Γ small, where the effect of U_q can be disregarded [empty red squares in Fig. 9(b)]. Therefore, we will consider this regime in the rest of the present Appendix and Fig. 10.

The use of a double quantum dot circuit as a nonlinear element for circuit QED can be interesting because it offers a strong tunability of the squeezing effect, as already seen in Fig. 9. Figure 10(a) shows that the amplitude of the squeezing effect is also strongly dependent on the average level position $\omega_{av} = (\omega_L + \omega_R)/2$. Besides, the squeezing effect can be controlled by using a nonzero bias voltage V_b [see Fig. 10(b)]. This is consistent with the fact mentioned earlier that using a nonzero V_b modifies the orbital energy range where the drive terms U_{cl} shows strong resonances [Figs. 3(a) and 3(c)]. Note that, so far, we have used a relatively high cavity damping rate Λ_0 which limits the squeezing effect. Figures 10(a) and 10(b) show that for a given set of double dot parameters, the squeezing effect increases when Λ_0 decreases, as expected. Finally, Fig. 9(d) shows an example of cavity Wigner function corresponding to the red empty circles in Fig. 9(c). Using the qutip package mesolve [81], we have checked that this Wigner function is in quantitative agreement with a direct numerical treatment of Eq. (46). We have also checked that fourth-order corrections in g_L are negligible for the parameters considered in the present section. Therefore, a treatment of the master equation (46) to third order in g_L is fully justified.

Interestingly, it has also been suggested to obtain cavity squeezing by using a single quantum dot with an ac excitation with amplitude ε'_p applied directly to the dot gate [44]. However, on the experimental level, such a strategy is more costly since it requires fabrication of a direct ac gate for the quantum dot. Note that Ref. [44] presents the cavity effective action to second order in g_L only. A coherent two-photon drive term in $\varepsilon'_p g_L^2$ is taken into account but the terms in χ_2, λ_2 and the expected contribution in $\varepsilon'_p g_L^2$ to U_q are disregarded. Alternatively, two-photon processes or photonic squeezing have been found for dc voltage-biased Josephson junctions or tunnel junctions, which have no internal degrees of freedom [45,46,89–91]. In our case, the dc voltage bias is not necessary due to the presence of the dot orbital degree of freedom.

APPENDIX G: ANALYTICAL EXPRESSION OF χ_2 FOR A DOUBLE QUANTUM DOT IN THE SEQUENTIAL TUNNELING LIMIT

In the sequential tunneling limit $k_B T \ll \Gamma$, it is possible to obtain a simple approximate expression of the charge susceptibility χ_2 for the double quantum dot of Sec. IV. One can use a semiclassical framework, with a master equation description of transport through the double quantum dot, and a resonant approximation between the double dot internal transition and the cavity. Such an approach is described in Sec. 4.2.1 of Ref. [18] and yields the expression

$$\chi_2 = \frac{2g_t^2(n_- - n_+)}{\omega_0 - \omega_{\rm DQD} + i\Gamma}. \tag{G1}$$

Above, the factor 2 takes into account spin degeneracy. The transverse coupling

$$g_t = (g_R - g_L)\sin[\theta]/2 \tag{G2}$$

between the DQD internal degree of freedom and the cavity depends on the mixing angle $\theta = \arctan[2t/(\varepsilon_L - \varepsilon_R)]$ between the left and right DQD orbitals. The average occupations n_- and n_+ of the bounding and antibounding orbitals of the DQD can be expressed as

$$n_+ = [2 - f_L^- - f_R^- + (f_L^- - f_R^-)\cos(\theta)] \times [f_L^+ + f_R^+ + (f_L^+ - f_R^+)\cos(\theta)]/4 \tag{G3}$$

and

$$n_- = [2 - f_L^+ - f_R^+ + (f_R^+ - f_L^+)\cos(\theta)] \times [f_L^- + f_R^- + (f_R^- - f_L^-)\cos(\theta)]/4 \tag{G4}$$

with $f_{L(R)}^\pm = \{1 + \exp[\pm(\omega_{L(R)} \mp (eV_b/2))/k_B T]\}^{-1}$.

Figure 11 shows a comparison between the values of χ_2 given by Eqs. (G1) and (30). The agreement is very good near the resonances $\omega_0 = \omega_{\rm DQD}$, provided $t_{LR} \gg \Gamma$, because Eq. (G1) disregards photoassisted tunneling to the normal metal contacts, contrary to Eq. (30). One interest of Eq. (G1) is that it shows explicitly that divergences of χ_2, which should occur for $\omega_0 = \omega_{\rm DQD}$ in the absence of dissipation, are regularized by the dissipative dot-lead tunneling in Γ. More generally, in our model, dissipative tunneling to the reservoirs prevents divergences of the cavity effective parameters, because it generates imaginary self-energy terms in the mesoscopic Green's function of Eq. (23). This is visible, for instance, in Figs. 3 and 4, which present the numerical evaluation of these parameters versus $\omega_{L(R)}$ or $\Delta\omega_{LR} = \omega_L - \omega_R$.

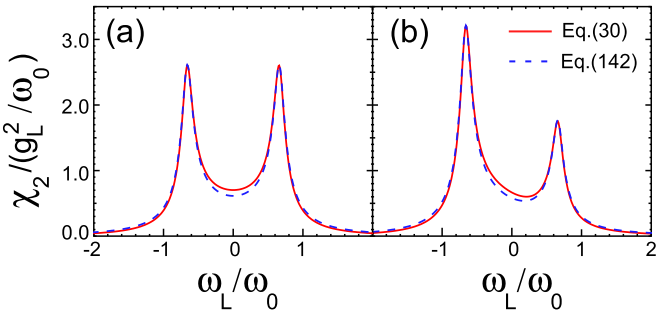

FIG. 11. Charge susceptibility χ_2 of the DQD of Sec. IV vs ω_L for $V_b = 0$ (a) and $V_b = 0.5\omega_0$ (b). The full red lines and dashed blue lines correspond to the result given by Eqs. (30) and (142), respectively. The other parameters used are $\omega_R = 0$, $\Gamma = 0.05\omega_0$, $t_{LR} = 0.375\omega_0$, $k_B T = 0.5\omega_0$, $g_R = 0$, and $V_b = 0.5\omega_0$.

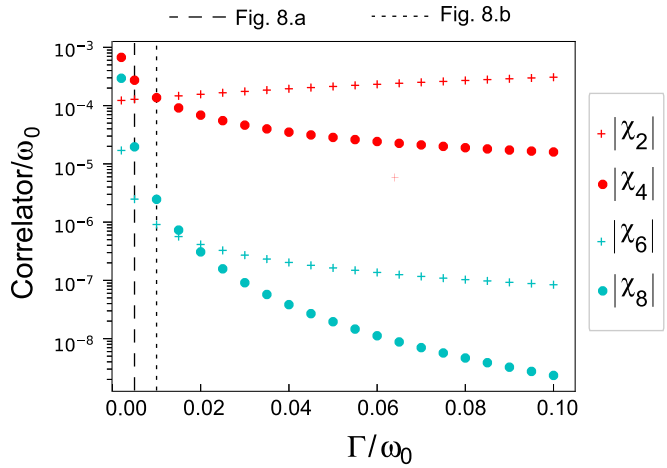

FIG. 12. Charge susceptibility coefficients χ_2, χ_4, χ_6, and χ_8 of the DQD of Sec. IV vs Γ for the parameters of Figs. 7 and 8. The vertical dashed lines indicate the values of Γ used in Figs. 8(a) and 8(b).

APPENDIX H: VALIDITY OF OUR PERTURBATION SCHEME FROM THE ESTIMATION OF HIGHER ORDER CORRELATORS IN g

Since we develop the cavity action with respect to $\check{g}$ and β_p, the amplitude of these two parameters must not be too large. Besides, having $\Gamma \neq 0$ is crucial for ensuring the validity of our perturbation scheme in the single- or two-photon resonant regimes. Indeed, in the absence of dissipation, the correlators χ_2 and χ_4 are expected to diverge at $\omega_{\rm DQD} = \omega_0$ and/or $\omega_{\rm DQD} = 2\omega_0$ [80]. However, giving a simple analytic criterion for the regime of validity of our description is very complex. Strictly speaking, the development parameter in our approach is the functional matrix $\check{m}$ of Eq. (A8), which is used in the development of the cavity effective action. It is difficult to express analytically a smallness criterion on this quantity due to the many parameters involved through Eqs. (27) and (A8) together with the light/matter coupling. This is why, out of conciseness, we have referred to the expansion parameter as g in the main text. One can check the validity of our development *a posteriori*, by estimating mesoscopic correlators which would occur in the cavity effective action at higher orders in g and β_p to check whether they are negligible. Here, we present the evaluation of the generalized charge susceptibilities χ_6 and χ_8 of the mesoscopic circuit at orders 6 and 8 in g respectively. We expect the other coefficients with the same order in g to have order of magnitudes similar to χ_6 and χ_8 at best, similarly to what we observe at orders 2 and 4 in g. The parameters χ_6 and χ_8 can be estimated from a semiclassical approach similar to that of Appendix B1. By analogy with Eqs. (29), (38), (B7), and (B10), one gets

$$S_{\rm cav}^{\rm eff}(\bar{\varphi}, \varphi) = \sum_{n\geqslant 1} (\bar{\varphi}_{cl}\varphi_{cl})^n \bar{\varphi}_q \varphi_{cl}\, \chi_{2n} + \cdots . \tag{H1}$$

Let us define

$$\tilde{G}^j_{r,n}(\omega) = \sum_{(a_1,a_2,a_{n-1})\in\mathcal{S}_n} [\mathcal{G}^r(\omega + j\omega_0)\tilde{g}\mathcal{G}^r(\omega + a_1\omega_0)\tilde{g}\mathcal{G}^r(\omega + a_2\omega_0)\ldots\tilde{g}\mathcal{G}^r(\omega + a_{n-1}\omega_0)\tilde{g}\mathcal{G}^r(\omega)],$$

where $\mathcal{S}_n$ is the ensemble of number sequences (a_1, a_2, a_{n-1}) such that $a_1 = j \pm 1$, $a_k - a_{k-1} = \pm 1$ for $k \in [2, n-1]$ and $a_{n-1} = \pm 1$. One can check

$$\chi_n(\omega_0) = -\frac{i}{2^{n-2}} Tr\left[\tilde{g} \sum_{\substack{i\in[0,n-1]\\ k_i + k_{n-i} = -1}} \int \frac{d\omega}{2\pi} \tilde{G}^{k_i}_{r,i}(\omega)\tilde{\Sigma}^<(\omega)\tilde{G}^{k_{n-i}}_{a,n-1-i}(\omega)\right]$$

with

$$\tilde{G}^j_{a,n}(\omega) = \left[\tilde{G}^{-j}_{r,n}(\omega)\right]^\dagger .$$

Figure 12 shows the absolute values of χ_2, χ_4, χ_6, and χ_8 versus Γ for the parameters of Figs. 7 and 8. For $\Gamma = 0.0025\omega_0$, $|\chi_8|$ has the same order of magnitude as $|\chi_2|$ and $|\chi_4|$. This illustrates the fact that our development in g^4 is not valid for too small values of Γ. However, for the values $\Gamma = 0.005\omega_0$ and $\Gamma = 0.01\omega_0$ corresponding to Figs. 8(a) and 8(b) (indicated by vertical dashed lines), one starts to have χ_2, $\chi_4 \gg \chi_6$, and χ_8 so that our development at fourth order in g seems reasonable. It turns out that we have worked at the limit of the allowed range of Γ in order to maximize the two-photons effects in $K_{\rm loss}$ which decrease for higher values of Γ (one has $K_{\rm loss} = {\rm Im}[\chi_4] \simeq -i\chi_4$ for the parameters of Fig. 8). We have checked that χ_2, $\chi_4 \gg \chi_6$, χ_8 is also satisfied for the parameters used in Sec. III and Appendix F. In principle, terms at higher orders in β_p should

also contribute to Eq. (H1). However, the next order contribution after the term in $\beta_p g^3$ of the main text should be in $\beta_p^2 g^6$ and since it is also regularized by Γ, we expect this term to be negligible.

[1] A. Wallraff, D. I. Schuster, A. Blais, L. Frunzio, R.- S. Huang, J. Majer, S. Kumar, S. M. Girvin and R. J. Schoelkopf, Strong coupling of a single photon to a superconducting qubit using circuit quantum electrodynamics, Nature (London) **431**, 162 (2004).

[2] F. Mallet, M. A. Castellanos-Beltran, H. S. Ku, S. Glancy, E. Knill, K. D. Irwin, G. C. Hilton, L. R. Vale, and K. W. Lehnert, Quantum State Tomography of an Itinerant Squeezed Microwave Field, Phys. Rev. Lett. **106**, 220502 (2011).

[3] G. Kirchmair, B. Vlastakis, Z. Leghtas, S. E. Nigg, H. Paik, E. Ginossar, M. Mirrahimi, L. Frunzio, S. M. Girvin, and R. J. Schoelkopf, Observation of quantum state collapse and revival due to the single-photon Kerr effect, Nature (London) **495**, 205 (2013).

[4] M. Hofheinz, E. M. Weig, M. Ansmann, Radoslaw C. Bialczak, Erik Lucero, M. Neeley, A. D. O'Connell, H. Wang, John M. Martinis, and A. N. Cleland, Generation of Fock states in a superconducting quantum circuit, Nature (London) **454**, 310 (2008).

[5] M. Hofheinz, H. Wang, M. Ansmann, R. C. Bialczak, E. Lucero, M. Neeley, A. D. O'Connell, D. Sank, J. Wenner, J. M. Martinis, and A. N. Cleland, Synthesizing arbitrary quantum states in a superconducting resonator, Nature (London) **459**, 546 (2009).

[6] Z. Leghtas, S. Touzard, I. M. Pop, A. Kou, B. Vlastakis, A. Petrenko, K. M. Sliwa, A. Narla, S. Shankar, M. J. Hatridge, M. Reagor, L. Frunzio, R. J. Schoelkopf, M. Mirrahimi, and M. H. Devoret, Confining the state of light to a quantum manifold by engineered two-photon loss, Science **347**, 853 (2015).

[7] S. Touzard, A. Grimm, Z. Leghtas, S. O. Mundhada, P. Reinhold, C. Axline, M. Reagor, K. Chou, J. Blumoff, K. M. Sliwa, S. Shankar, L. Frunzio, R. J. Schoelkopf, M. Mirrahimi, and M. H. Devoret, Coherent Oscillations Inside a Quantum Manifold Stabilized by Dissipation, Phys. Rev. X **8**, 021005 (2018).

[8] E. T. Holland, B. Vlastakis, R. W. Heeres, M. J. Reagor, U. Vool, Z. Leghtas, L. Frunzio, G. Kirchmair, M. H. Devoret, M. Mirrahimi, and R. J. Schoelkopf, Single-Photon Resolved Cross-Kerr Interaction for Autonomous Stabilization of Photon-Number States, Phys. Rev. Lett. **115**, 180501 (2015).

[9] J. F. Poyatos, J. I. Cirac, and P. Zoller, Quantum Reservoir Engineering with Laser Cooled Trapped Ions, Phys. Rev. Lett. **77**, 4728 (1996).

[10] A. Sarlette, Z. Leghtas, M. Brune, J. M. Raimond, and P. Rouchon, Stabilization of nonclassical states of one- and two-mode radiation fields by reservoir engineering, Phys. Rev. A **86**, 012114 (2012).

[11] C. Aron, M. Kulkarni, and H. E. Türeci, Steady-state entanglement of spatially separated qubits via quantum bath engineering, Phys. Rev. A **90**, 062305 (2014).

[12] A. Roy, Z. Leghtas, A. D. Stone, M. Devoret, and M. Mirrahimi, Continuous generation and stabilization of mesoscopic field superposition states in a quantum circuit, Phys. Rev. A **91**, 013810 (2015).

[13] C. M. Caves, K. S. Thorne, R. W. P. Drever, V. D. Sandberg, and M. Zimmermann, On the measurement of a weak classical force coupled to a quantum-mechanical oscillator, Rev. Mod. Phys. **52**, 341 (1980).

[14] V. Giovannetti, S. Lloyd, and L. Maccone, Quantum-enhanced measurements: Beating the standard quantum limit, Science **306**, 1330 (2004).

[15] M. Mirrahimi, Z. Leghtas, V. V. Albert, S. Touzard, R. J. Schoelkopf, L. Jiang and M. H. Devoret, Dynamically protected cat-qubits: A new paradigm for universal quantum computation, New J. Phys. **16**, 045014 (2014).

[16] S. Haroche and J.-M. Raimond, *Exploring the Quantum: Atoms, Cavities, and Photons*, Oxford Graduate Texts (Oxford University Press, Oxford, UK, 2006).

[17] B. Reulet, M. Ramin, H. Bouchiat, and D. Mailly, Dynamic Response of Isolated Aharonov-Bohm Rings Coupled to an Electromagnetic Resonator, Phys. Rev. Lett. **75**, 124 (1995).

[18] A. Cottet, M. C. Dartiailh, M. M. Desjardins, T. Cubaynes, L. C. Contamin, M. Delbecq, J. J. Viennot, L. E. Bruhat, B. Douçot, and T. Kontos, Cavity QED with hybrid nanocircuits: From atomic-like physics to condensed matter phenomena, J. Phys.: Condens. Matter **29**, 433002 (2017).

[19] M. R. Delbecq, V. Schmitt, F. D. Parmentier, N. Roch, J. J. Viennot, G. Fève, B. Huard, C. Mora, A. Cottet, and T. Kontos, Coupling a Quantum Dot, Fermionic Leads, and a Microwave Cavity On-Chip, Phys. Rev. Lett. **107**, 256804 (2011).

[20] T. Frey, P. J. Leek, M. Beck, A. Blais, T. Ihn, K. Ensslin, and A. Wallraff, Dipole Coupling of a Double Quantum Dot to a Microwave Resonator, Phys. Rev. Lett. **108**, 046807 (2012).

[21] J. J. Viennot, M. C. Dartiailh, A. Cottet, and T. Kontos, Coherent coupling of a single spin to microwave cavity photons, Science **349**, 408 (2015).

[22] T. Cubaynes, M. R. Delbecq, M. C. Dartiailh, R. Assouly, M. M. Desjardins, L. C. Contamin, L. E. Bruhat, Z. Leghtas, F. Mallet, A. Cottet, and T. Kontos, Highly coherent spin states in carbon nanotubes coupled to cavity photons, npj Quant. Inf. **5**, 47 (2019).

[23] L. E. Bruhat, J. J. Viennot, M. C. Dartiailh, M. M. Desjardins, T. Kontos, and A. Cottet, Cavity Photons as a Probe for Charge Relaxation Resistance and Photon Emission in a Quantum Dot Coupled to Normal and Superconducting Continua, Phys. Rev. X **6**, 021014 (2016).

[24] L. E. Bruhat, T. Cubaynes, J. J. Viennot, M. C. Dartiailh, M. M. Desjardins, A. Cottet, and T. Kontos, Circuit QED with a quantum-dot charge qubit dressed by Cooper pairs, Phys. Rev. B **98**, 155313 (2018).

[25] X. Mi, J. V. Cady, D. M. Zajac, P. W. Deelman, and J. R. Petta, Strong coupling of a single electron in silicon to a microwave photon, Science **355**, 156 (2017).

[26] A. Stockklauser, P. Scarlino, J. V. Koski, S. Gasparinetti, C. K. Andersen, C. Reichl, W. Wegscheider, T. Ihn, K. Ensslin, and A. Wallraff, Strong Coupling Cavity QED with Gate-Defined Double Quantum Dots, Phys. Rev. X **7**, 011030 (2017).

[27] X. Mi, M. Benito, S. Putz, D. M. Zajac, J. M. Taylor, G. Burkard, and J. R. Petta, A coherent spin-photon interface in silicon, Nature (London) **555**, 599 (2018).

[28] N. Samkharadze, G. Zheng, N. Kalhor, D. Brousse, A. Sammak, U. C. Mendes, A. Blais, G. Scappucci, and L. M. K.

Vandersypen, Strong spin-photon coupling in silicon, Science **359**, 1123 (2018).

[29] A. J. Landig, J. V. Koski, P. Scarlino, U. C. Mendes, A. Blais, C. Reichl, W. Wegscheider, A. Wallraff, K. Ensslin, and T. Ihn, Coherent spin-qubit photon coupling, Nature (London) **560**, 179 (2018).

[30] M. Schiró and K. Le Hur, Tunable hybrid quantum electrodynamics from nonlinear electron transport, Phys. Rev. B **89**, 195127 (2014).

[31] O. Dmytruk, M. Trif, and P. Simon, Cavity quantum electrodynamics with mesoscopic topological superconductors, Phys. Rev. B **92**, 245432 (2015).

[32] O. Dmytruk, M. Trif, C. Mora, and P. Simon, Cavity quantum electrodynamics with an out-of-equilibrium quantum dot, Phys. Rev. B **93**, 075425 (2016).

[33] M. C. Dartiailh, T. Kontos, B. Douçot, and A. Cottet, Direct Cavity Detection of Majorana Pairs, Phys. Rev. Lett. **118**, 126803 (2017).

[34] P.-Q. Jin, M. Marthaler, J. H. Cole, A. Shnirman, and G. Schön, Lasing and transport in a quantum-dot resonator circuit, Phys. Rev. B **84**, 035322 (2011).

[35] P.-Q. Jin, M. Marthaler, J. H. Cole, A. Shnirman, and G. Schön, Lasing and transport in a coupled quantum dot-resonator system, Phys. Scr. **T151**, 014032 (2012).

[36] P.-Q. Jin, M. Marthaler, P.-Q. Jin, D. Golubev and G. Schön, Noise spectrum of a quantum dot-resonator lasing circuit, New J. Phys. **15**, 025044 (2013).

[37] M. Kulkarni, O. Cotlet, and H. E. Türeci, Cavity-coupled double-quantum dot at finite bias: Analogy with lasers and beyond, Phys. Rev. B **90**, 125402 (2014).

[38] A. Stockklauser, V. F. Maisi, J. Basset, K. Cujia, C. Reichl, W. Wegscheider, T. Ihn, A. Wallraff, and K. Ensslin, Microwave Emission from Hybridized States in a Semiconductor Charge Qubit, Phys. Rev. Lett. **115**, 046802 (2015).

[39] J. J. Viennot, M. R. Delbecq, M. C. Dartiailh, A. Cottet, and T. Kontos, Out of equilibrium charge dynamics in a hybrid cQED architecture, Phys. Rev. B **89**, 165404 (2014).

[40] A. Kamenev, *Field Theory of Non-equilibrium Systems* (Cambridge University Press, Cambridge, UK, 2011).

[41] D. F. Walls and G. J. Milburn, *Quantum Optics*, 2nd ed. (Springer, Berlin, 2008).

[42] N. Didier, F. Qassemi, and A. Blais, Perfect squeezing by damping modulation in circuit quantum electrodynamics, Phys. Rev. A **89**, 013820 (2014).

[43] X.-Y. Lü, Y. Wu, J. R. Johansson, H. Jing, J. Zhang, and F. Nori, Squeezed Optomechanics with Phase-Matched Amplification and Dissipation, Phys. Rev. Lett. **114**, 093602 (2015).

[44] U. C. Mendes and C. Mora, Cavity squeezing by a quantum conductor, New J. Phys. **17**, 113014 (2015).

[45] U. C. Mendes and C. Mora, Electron-photon interaction in a quantum point contact coupled to a microwave resonator, Phys. Rev. B **93**, 235450 (2016).

[46] A. L. Grimsmo, F. Qassemi, B. Reulet, and A. Blais, Quantum Optics Theory of Electronic Noise in Coherent Conductors, Phys. Rev. Lett. **116**, 043602 (2016).

[47] S. Puri, S. Boutin, and A. Blais, npj Quantum Inf. **3**, 18 (2017).

[48] A. Grimm, N. E. Frattini, S. Puri, S. O. Mundhada, S. Touzard, M. Mirrahimi, S. M. Girvin, S. Shankar, and M. H. Devoret, The Kerr-cat qubit: Stabilization, readout, and gates, Nature (London) **584**, 205 (2020).

[49] S. Puri, L. St-Jean, J. A. Gross, A. Grimm, N. E. Frattini, P. S. Iyer, A. Krishna, S. Touzard, L. Jiang, A. Blais, S. T. Flammia, and S. M. Girvin, Bias-preserving gates with stabilized cat qubits, Science Advances **6**, eaay5901 (2020).

[50] R. Lescanne, M. Villiers, T. Peronnin, A. Sarlette, M. Delbecq, B. Huard, T. Kontos, M. Mirrahimi, and Z. Leghtas, Exponential suppression of bit-flips in a qubit encoded in an oscillator, Nat. Phys. **16**, 509 (2020).

[51] V. Mourik, K. Zuo, S. M. Frolov, S. R. Plissard, E. P. A. M. Bakkers, and L. P. Kouwenhoven, Signatures of Majorana fermions in hybrid superconductor-semiconductor nanowire devices, Science **336**, 1003 (2012).

[52] A. Das, Y. Ronen, Y. Most, Y. Oreg, M. Heiblum, and H. Shtrikman, Zero-bias peaks and splitting in an Al-InAs nanowire topological superconductor as a signature of Majorana fermions, Nat. Phys. **8**, 887 (2012).

[53] M. T. Deng, C. L. Yu, G. Y. Huang, M. Larsson, P. Caroff, and H. Q. Xu, Anomalous zero-bias conductance peak in a Nb-InSb nanowire-Nb hybrid device, Nano Lett. **12**, 6414 (2012).

[54] H. O. H. Churchill, V. Fatemi, K. Grove-Rasmussen, M. T. Deng, P. Caroff, H. Q. Xu, and C. M. Marcus, Superconductor-nanowire devices from tunneling to the multichannel regime: Zero-bias oscillations and magnetoconductance crossover, Phys. Rev. B **87**, 241401(R) (2013).

[55] S. M. Albrecht, A. P. Higginbotham, M. Madsen, F. Kuemmeth, T. S. Jespersen, J. Nygård, P. Krogstrup, and C. M. Marcus, Exponential protection of zero modes in Majorana islands, Nature (London) **531**, 206 (2016).

[56] Ö. Gül, H. Zhang, J. D. S. Bommer, M. W. A. de Moor, D. Car, S. R. Plissard, E. P. A. M. Bakkers, A. Geresdi, K. Watanabe, T. Taniguchi, and L. P. Kouwenhoven, Ballistic Majorana nanowire devices, Nat. Nanotechnol. **13**, 192 (2018)

[57] L. Tosi, C. Metzger, M. F. Goffman, C. Urbina, H. Pothier, Sunghun Park, A. L. Yeyati, J. Nygård, and P. Krogstrup, Spin-Orbit Splitting of Andreev States Revealed by Microwave Spectroscopy, Phys. Rev. X **9**, 011010 (2019).

[58] M. Trif and Y. Tserkovnyak, Resonantly Tunable Majorana Polariton in a Microwave Cavity, Phys. Rev. Lett. **109**, 257002 (2012).

[59] T. L. Schmidt, A. Nunnenkamp, and C. Bruder, Majorana Qubit Rotations in Microwave Cavities, Phys. Rev. Lett. **110**, 107006 (2013).

[60] A. Cottet, T. Kontos, and B. Douçot, Squeezing light with Majorana fermions, Phys. Rev. B **88**, 195415 (2013).

[61] A. Cottet, T. Kontos, and A. L. Yeyati, Subradiant Split Cooper Pairs, Phys. Rev. Lett. **108**, 166803 (2012).

[62] A. Cottet, Probing coherent Cooper pair splitting with cavity photons, Phys. Rev. B **90**, 125139 (2014).

[63] M. Mantovani, W. Belzig, G. Rastelli, and R. Hussein, Single-photon pump by Cooper-pair splitting, Phys. Rev. Res. **1**, 033098 (2019).

[64] Y.-Y. Liu, J. Stehlik, C. Eichler, M. J. Gullans, J. M. Taylor, and J. R. Petta, Semiconductor double quantum dot micromaser, Science **347**, 285 (2015).

[65] G. Rastelli and M. Governale, Single atom laser in normal-superconductor quantum dots, Phys. Rev. B **100**, 085435 (2019).

[66] M. M. Desjardins, J. J. Viennot, M. C. Dartiailh, L. E. Bruhat, M. R. Delbecq, M. Lee, M.-S. Choi, A. Cottet and T. Kontos,

Observation of the frozen charge of a Kondo resonance, Nature (London) **545**, 71 (2017).

[67] A. C. Hewson and D. Meyer, Numerical renormalization group study of the Anderson-Holstein impurity model, J. Phys.: Condens. Matter **14**, 427 (2002).

[68] A. Cottet, T. Kontos, and B. Douçot, Electron-photon coupling in mesoscopic quantum electrodynamics, Phys. Rev. B **91**, 205417 (2015).

[69] M. Benito, X. Mi, J. M. Taylor, J. R. Petta, and G. Burkard, Input-output theory for spin-photon coupling in Si double quantum dots, Phys. Rev. B **96**, 235434 (2017).

[70] K. Blum, *Density Matrix Theory and Applications*, 3rd ed. (Springer, Berlin, 2012).

[71] R. Zamoum, M. Lavagna, and A. Crépieux, Nonsymmetrized noise in a quantum dot: Interpretation in terms of energy transfer and coherent superposition of scattering paths, Phys. Rev. B **93**, 235449 (2016).

[72] More mathematically speaking, $\varphi_\pm(t)$ and $\psi_{\pm,d}(t)$ represent eigenvalues of the operators $\hat{a}$ and $\hat{c}_d$ in a coherent eigenstate picture where one can use $\hat{a}|\varphi_\pm(t)\rangle = \varphi_\pm(t)|\varphi_\pm(t)\rangle$ and $\hat{c}_d|\psi_{\pm,d}(t)\rangle = \psi_{\pm,d}(t)|\psi_{\pm,d}(t)\rangle$. Details on the construction of this representation are given in Refs. [40,86].

[73] E. G. D. Torre, S. Diehl, M. D. Lukin, S. Sachdev, and P. Strack, Keldysh approach for nonequilibrium phase transitions in quantum optics: Beyond the Dicke model in optical cavities, Phys. Rev. A **87**, 023831 (2013).

[74] A. Cottet, C. Mora, and T. Kontos, Mesoscopic admittance of a double quantum dot, Phys. Rev. B **83**, 121311(R) (2011).

[75] In Refs. [42,43], a squeezing superoperator form $\mathcal{S}_{\hat{L}_j}(\rho^I_{\rm cav}) = \hat{L}_j\rho^I_{\rm cav}\hat{L}_j - \frac{1}{2}\{\hat{L}_j\hat{L}_j, \rho^I_{\rm cav}\}$ is used on top of the standard superoperator form $L_{\hat{L}_j}$ defined in our Eq. (13). In this framework, the dissipation term $\gamma_{\rm loss}\mathcal{D}_{\hat{a}} + \gamma_{\rm gain}\mathcal{D}_{\hat{a}} + \gamma_p\mathcal{D}_{\hat{a}+e^{i\varphi_p}\hat{a}^\dagger}$, which appears in the right-hand side of Eq. (67), can be rewritten as $\gamma^0_{\rm loss}\mathcal{D}_{\hat{a}} + \gamma^0_{\rm gain}\mathcal{D}_{\hat{a}} + \gamma_p e^{i\varphi_p}\mathcal{S}_{\hat{a}^\dagger} + \gamma_p e^{-i\varphi_p}\mathcal{S}_{\hat{a}}$.

[76] This is possible provided the capacitances to the source and drain contacts are equal and the capacitance between the two dots is very large. In the general case, our results will remain valid provided $\omega_{L(R)}$ are understood as V-shifted orbital energies.

[77] A.-P. Jauho, N. S. Wingreen, and Y. Meir, Time-dependent transport in interacting and noninteracting resonant-tunneling systems, Phys. Rev. B **50**, 5528 (1994).

[78] V. Talbo, M. Lavagna, T. Q. Duong, and A. Crépieux, Charge susceptibility and conductances of a double quantum dot, AIP Adv. **8**, 101333 (2018).

[79] N. Samkharadze, A. Bruno, P. Scarlino, G. Zheng, D. P. DiVincenzo, L. DiCarlo, and L. M. K. Vandersypen, High-Kinetic-Inductance Superconducting Nanowire Resonators for Circuit QED in a Magnetic Field, Phys. Rev. Appl. **5**, 044004 (2016).

[80] In the absence of leads in the DQD circuit, one can calculate $\Delta\omega_0 = \mathrm{Re}[\chi_2]$ and $K = \mathrm{Re}[\chi_4]$ by performing an adiabatic elimination, or Schrieffer Wolf transformation [92], to calculate $\Delta\omega_0 = \mathrm{Re}[\chi_2]$ and $K = \mathrm{Re}[\chi_4]$. One finds that $\Delta\omega_0$ has a denominator in $\omega_0^2 - \omega_{\rm DQD}^2$ and K has a denominator in $(\omega_0^2 - \omega_{\rm DQD}^2)^3(4\omega_0^2 - \omega_{\rm DQD}^2)$ (see detailed formulas in Ref. [60], Eqs. (12)–(14), which are valid for a closed two-level system coupled to a cavity). Therefore, $\Delta\omega_0$ diverges for $\omega_0 = \pm\omega_{\rm DQD}$ and K for $\omega_0 = \pm\omega_{\rm DQD}$ and $\omega_0 = \pm 2\omega_{\rm DQD}$.

[81] J. R. Johansson, P. D. Nation, and F. Nori, QuTiP: An open-source Python framework for the dynamics of open quantum systems, Comput. Phys. Commun. **183**, 1760 (2012).

[82] C. Müller and T. M. Stace, Deriving Lindblad master equations with Keldysh diagrams: Correlated gain and loss in higher order perturbation theory, Phys. Rev. A **95**, 013847 (2017).

[83] S. Gustavsson, R. Leturcq, B. Simovič, R. Schleser, T. Ihn, P. Studerus, K. Ensslin, D. C. Driscoll, and A. C. Gossard, Counting Statistics of Single Electron Transport in a Quantum Dot, Phys. Rev. Lett. **96**, 076605 (2006).

[84] R. Azouit, F. Chittaro, A. Sarlette, and P. Rouchon, Towards generic adiabatic elimination for bipartite open quantum systems, Quantum Sci. Technol. **2**, 044011 (2017).

[85] P. Forni, A. Sarlette, T. Capelle, E. Flurin, S. Deléglise, and P. Rouchon, Adiabatic elimination for multipartite open quantum systems with nontrivial zero-order dynamics, arXiv:1803.07810.

[86] J. Zinn-Justin, *Path Integrals in Quantum Mechanics*, Oxford Graduate Texts (Oxford University Press, Oxford, UK, 2004).

[87] See Eq. (2.44) and Sec. 9.3 of Ref. [40] and the definition (26) of $\tilde{G}_K^{d,d}$.

[88] L. M. Sieberer, M. Buchhold, and S. Diehl, Keldysh field theory for driven open quantum systems, Rep. Prog. Phys. **79**, 096001 (2016).

[89] G. Gasse, C. Lupien, and B. Reulet, Observation of Squeezing in the Electron Quantum Shot Noise of a Tunnel Junction, Phys. Rev. Lett. **111**, 136601 (2013).

[90] J.-C. Forgues, C. Lupien, and B. Reulet, Experimental Violation of Bell-Like Inequalities by Electronic Shot Noise, Phys. Rev. Lett. **114**, 130403 (2015).

[91] M. Westig, B. Kubala, O. Parlavecchio, Y. Mukharsky, C. Altimiras, P. Joyez, D. Vion, P. Roche, D. Esteve, M. Hofheinz, M. Trif, P. Simon, J. Ankerhold, and F. Portier, Emission of Non-Classical Radiation by Inelastic Cooper Pair Tunneling, Phys. Rev. Lett. **119**, 137001 (2017).

[92] C. Cohen-Tannoudji, J. Dupont-Roc, and G. Grynberg, *Atom-Photon Interactions: Basic Processes and Applications* (Wiley, New York, 1992).